Reinforcement of ice covers for transportation: beam and preliminary plate testing

Barrette, Paul D.

Publisher's version / Version de l'éditeur:
https://doi.org/10.4224/8894844
Technical Report (National Research Council of Canada. Ocean, Coastal and River Engineering); no. NRC-OCRE-2019-TR-034, 2020-02-14

NRC·CNRC

Reinforcement of ice covers for transportation: Beam and preliminary plate testing

NRC-OCRE-2019-TR-034

Revision 7.0
February 14, 2020

Prepared for:
Transport Canada
Crown-Indigenous Relations and Northern Affairs (CIRNAC)
NRC Arctic Program

Author:
Paul D. Barrette

Ocean, Coastal, and River Engineering
Research Centre

National Research Council Canada
Conseil national de recherches Canada

Canada

Revision History

Document Version	Name	Affiliation	Date of Changes	Comments
1.0	Bob Frederking	NRC-OCRE	Nov. 4, 2019	First draft – Sections 1 and 2
3.0	Hossein Babaei	NRC-OCRE	Dec. 22, 2019	Section 3
4.0	Denise Sudom	NRC-OCRE	Dec. 23, 2019	General overview
5.0	Anne Barker	NRC-OCRE	Jan. 29, 2020	General overview

Cat. No. NR16-289/1-2020E-PDF
ISBN 978-0-660-34295-5

Summary

Winter road networks generally comprise segments that run over land and/or over floating ice expanses (rivers and lakes). The latter commonly are weak links in these operations, because they rely on cold temperatures to achieve a thickness that is safe enough for the intended traffic. These are thus vulnerable to warmer air temperatures. Risks of breakthroughs are also a serious consideration. One option is to increase the predictability of these over-ice segments as well as their ability to support a load and resist failure. This may be achieved if the ice cover is artificially reinforced. A laboratory study, building on past investigations by other research groups, was conducted to provide additional information on this topic and also to guide a follow-up plate testing program. Four-point beam bending tests were conducted on freshwater ice without and with reinforcement, for comparison purposes. Threaded steel rods, a steel mesh and a polypropylene geogrid were used as reinforcement material. In all tests, the load and the loading rate increases with time up to a peak load. For the non-reinforced ice, there is a sudden drop in load at which point the tests end. For the reinforced ice, a drop in load also follows the peak load, but the load climbs again up to another peak in a repetitive fashion, so as to produce a saw tooth pattern, extending to a significant amount of time. The ice reinforced with the threaded rods had the highest resistance (exceeding the load cell capacity). Thin section observations showed that the crystal structure was forming around the material. However, cleavage surfaces along the ice/material interface after beam failure indicate that the interface could be a strength reduction factor.

Following the aforementioned, plate testing was also conducted to confirm these findings. Steel cables and a polypropylene geogrid were used as reinforcement, with non-reinforced and reinforced simply supported circular ice plates, as well as in a non-rotational mode. Testing was displacement-controlled, with a displacement rate of 1.4 mm per second. Instrumentation included a load cell, displacement transducers and an acoustic sensor to get information on cracking activity. Video sequences of each event yielded key information on plate response. It was correlated with the data from the instruments' output. Elastic deformation and cracking activity were generated. A good correlation existed between the response of the vertical load and cracking activity under a constant downward displacement rate. All plates failed via radial cracking, early in the loading event. The ice without reinforcement did so catastrophically. In contrast, for tests with reinforcement, the initial cracking activity was followed by on-going development of crack networks, including along the interface between the ice and the reinforcement material, indicating the material itself was a crack nucleation site. Acoustic emission recorded the evolution of all cracking activity and provides an opportunity to quantify the amount of energy absorbed by the ice plates during the loading event.

Proposed follow-up to this work includes: further plate testing, analyses of the short-term loading response, numerical modeling of the elastic response, a closer look at the correspondence between the visual observations and instrument output, a detailed analysis of the acoustic emission, and the preliminary assessment of field deployment.

Table of Contents

1. Introduction

An ice cover refers to a frozen water surface – a lake, a river, a sea expanse – that is floating on the underlying water. Once it has grown down to a sufficient thickness, it becomes a very practical platform (horizontal and mostly flat) for surface transportation during the winter months. A safe ice cover is one where the buoyancy of the ice and its mechanical resistance provide the necessary support without failing, that is, without crack development, since these can lead to breakthrough. Most winter roads – seasonal roads used only in the winter – comprise segments that run over ice covers, often referred to as 'ice roads', 'ice crossings' or 'ice bridges'. Such segments are commonly a limiting factor in a winter road operation. The reason is that, before opening, the ice needs to achieve a target thickness, one that is safe enough for the intended traffic. In the years during which the air temperatures are higher than normal, this has important implications. Namely:

1. The road will open later, delaying the delivery of critical supplies to northern communities. In the meantime, some users will expect the ice to be trafficable and will be tempted to use the ice without being fully aware it is unsafe, thereby increasing the risks of breakthroughs.
2. Mid-season closures and final closure due to a surface that has become too soft.

Most engineering materials used today (e.g. steel, metals and alloys, ceramics, concrete, asphalt, plastics and other organic synthetic compounds) are 'human-made' and, consequently, their properties are relatively homogeneous. This makes their mechanical behavior predictable. In the context of winter roads, ice is also considered an engineering material. But it is produced and controlled by nature, which does not promote uniformity. For instance, ice covers are typically made from layers of different densities and do not have a constant thickness across them. They also have an extensive, random network of internal cracks. Moreover, ice growth, natural or via artificial flooding and/or spray icing is only possible if the air temperature is low enough. At times, it is not.

One solution to this challenge is to incorporate an engineered material into the ice cover. This will achieve a number of goals:

1. It will increase the bearing capacity of the ice.
2. It will do so in a predictable fashion.
3. Even if the ice does fail (i.e. via fracturing), the engineered material inside the ice would support the load, thereby preventing breakthrough.
4. This material would become a tool available for operators to strengthen known weak links and prevent these locations from shortening the road's yearly operational lifespan.

Drawing from work done in the past by various research groups, the idea in this project was to identify a target reinforcement material, test it in the laboratory and generate enough information on its performance to guide prospective follow-up work in the form of one or more pilot studies in the field.

1.1. Climate change

Climate change has been held responsible for a downward trend, over the last number of decades, in the maximum annual ice thickness achieved during a given year, and the number of freezing-degree days (FDD)[1]. A large number of studies have been done on that topic (RSI, 2014, Hori et al., 2017, Hori and Gough, 2018). Figure 1 and Figure 2 provide an example of these trends. A warming climate is thought to increase the frequency and extent of warm winters. As such, it affects the safety and effectiveness of the winter road infrastructure and reduces its yearly operational lifespan. Contractors and engineering consultants have a wealth of knowledge and experience, and resort to various corrective measures to address the issues causing road closures. Ice growth via artificial flooding and/or spray icing are common techniques, but these are becoming insufficient.

1.2. Ice reinforcement

Incorporating an engineered material – an adequate geomembrane, geotextile, geogrid[2], or any other types of reinforcement - into an ice cover (Figure 3) is not a new concept. It has been investigated in the past century, including in the early 1940's, with the unlikely proposal to construct a floating anti-submarine base out of ice and wood pulp – the Habbakuk project (Gold, 2004). Since then, a variety of reinforcing materials have been incorporated in ice to improve its resilience – a summary of that work is presented elsewhere (Barrette, 2015).

1.3. Purpose of this report

This report is meant to summarize progress during Fiscal Year 2019-20 – it follows up on an earlier report (Barrette et al., 2019). It describes the outcome of two new series of laboratory tests: one with rectangular ice beams (Phase 1), the other with ice plates (Phase 2). The difference between the two test set-ups is schematized in Figure 4. Phase 1 testing is a 2D representation of the ice response in nature, i.e. the deformation takes place within a vertical plane. It is an extension of a preliminary stage described in the earlier report. Phase 2 test series is a 3D representation of the ice response, since it is taking into account the full surficial extent of the ice cover.

1.4. Rationale

The testing done with the two set-ups shown in Figure 4 are complementary approaches. Beam testing is easiest to implement, it requires less resources on a per-test basis, and its outcome can be used as guidance to plate testing. The latter is more representative of real scenarios, it allows an investigation of larger simulations with thicker ice, and is able to address deployment aspects. For both types of testing, information on loading mode and deformational response, in the context of winter roads, is presented elsewhere (Barrette, 2015).

1.5. Ice failure versus ice breakthrough

It is important to distinguish two terms – *ice failure* and *ice breakthrough* – because they have different consequences from an operational standpoint (for additional information about all operational aspects, the reader is referred to Government of the NWT, 2015). Both will be investigated in this project. The following is a description of how these terms are used in this report.

1.5.1. Resistance to ice failure (to 'first crack')

[1] FDDs is the average number of degrees below freezing point summed over the total number of days in a given time period. For instance, if the average air temperature on day 1, 2 and 3 was -5ºC, -8ºC and -12ºC, respectively, the number of FDD for these three days is 25ºC (5+8+12).

[2] These terms are here assumed to be synonymous. The prefix 'geo' refers to the most common deployment context (geotechnical engineering).

The term *ice failure* assumes a perfect elastic response and implies the formation of a 'first crack', i.e. the initial cracking activity in the ice. That notion is a simplification of reality, but it is helpful in understanding the ice response to vertical loading. For application to a real ice operation, this failure may allow the water to seep its way upward through the ice cover, resulting in a 'wet crack', causing local flooding on the ice surface. At that point, the ice cover is deemed unsafe. It is closed to traffic and may be flooded, until the ice freezes again In the meantime, if there is enough room, an alternative routing is built around that zone. The guidelines for the determination of a safe ice cover thickness are based on first crack.

As will be seen later in this report, beam and plate response varies according to whether or not it is reinforced. For non-reinforced ice, failure occurs at maximum load; for reinforced ice, several peaks in the load response are observed – the first one would presumably correspond to first crack in the context of a loaded ice cover. This will be discussed later.

1.5.2. Resistance to ice breakthrough, work and resilience

In a real scenario, *ice breakthrough* is beyond failure, and basically refers to the collapse of the ice cover at the point of load application. For a breakthrough to occur, the vertical weight exerted on it is sufficient not only to achieve first crack, but also to cause the vehicle (the person, an object, etc.) to go through the ice, either partially (e.g. one vehicle axle) or fully. It is the ultimate and unfortunate outcome of an ice cover that is unable to support the load, and may lead to injury or death. This breakthrough is expected to occur after a network of cracks has developed in the ice, namely tangential and circumferential. The energy expended in generating this crack network is referred in this report as *work*, and the resistance to breakthrough is referred to as *resilience* (*i.e.* the amount of work the ice can absorbed before breakthrough).

1.5.3. The role of reinforced ice

As indicated earlier (and discussed later), ice reinforcement has the capability of addressing both responses (failure and breakthrough), depending on the nature of the material used for that purpose. Provided the material adheres well to the ice and has an elastic modulus[3] higher than that of ice, it can improve the resistance to ice failure (i.e. resistance to first crack). If, as expected from any reinforcing material, it does not itself yield, then it will not only improve resistance to ice breakthrough *but will also prevent it*. What this means is that, even after sustaining extensive cracking, a reinforced ice cover can still play a critical role in preventing a vehicle from going through the ice.

[3] The elastic modulus represents the ability of the material to resist elastic deformation. A good analogy is a spring coil: a stiff coil (higher modulus) will require more force to extend then for a soft coil (lower modulus).

2. General principles on the deformation of ice covers

Unlike for most structures used by humans (buildings, bridges, ships, dams, etc.), ice covers over lakes, rivers and seas are produced by nature. We have limited control over that ice. The main concern is to be able to achieve a sufficient thickness for safe travel over it. For many operations where this is an issue, it is possible to increase thickness by using pumps to flood the ice and allowing this water to freeze. This increases ice thickness and, therefore, the ability of the ice cover to sustain higher loads. Another parameter controlled by nature is the internal structure (i.e. crystal size and internal layering). In general, this parameter is relatively uniform.

Yet another important consideration is that ice is, technically, a high temperature material, in the sense that it naturally exists very close to its melting temperature. In a previous report (Barrette, 2015), information was provided explaining why that is important. *For the purpose of the present report*, we will only retain that, because it is a high temperature material, only a small part of the deformation is elastic – other deformation mechanisms also operate. However, in ice engineering, it is customary to simplify the analyses by only addressing the elastic behavior, and assuming the ice is homogeneous. The analyses can then be pushed further by addressing micro-cracking, fracturing and breakthrough.

3. First phase: Beam testing

The earlier report on this project (Barrette et al. , 2019) provides an account of materials that could be used for reinforcement, and the parameters to be considered for a proper candidate selection. It also includes the outcome of a preliminary beam testing stage conducted in a cold room. That preliminary stage had a dual purpose:

- To procure and commission the required instrumentation and design testing procedures.
- To obtain some preliminary information on the mechanical response of ice beams that incorporated a reinforcement.

The formal beam testing stage, presented herein, is an extension of the preliminary stage. Additional beam testing was done on ice enclosing selected reinforcement materials, to supplement the information already gathered during the first stage. They are referred to herein as the R-series. As before, ice *without* reinforcement was also tested, for comparison purposes – they are referred to as the N-series.

3.1. Objectives

Two fundamental questions are being addressed:

- Does reinforcement increase beam resistance to ice failure? By resistance, we mean the load required to reach first crack (before reaching breakthrough).
- Does reinforcement increase beam resilience to failure? By resilience, we mean the energy required to break the beam (corresponding to breakthrough).

The reader is referred back to Section 1.5.1 for an explanation of what is meant here by ‘failure’ and ‘breakthrough’.

3.2. Methodology

All tests were done using OCRE’s cold room facilities in St. John’s. The methodology used for the new follow-up beam testing work was similar that used at the preliminary stage. All procedures are presented in the following, which includes some improvements and fine-tuning over the preliminary stage testing.

3.2.1. Ice production

Tap water was used for the production of the test specimens. The ice was grown in a basin 1600 mm in length, 600 mm in width and 520 mm in depth (Figure 5) inside an environmental chamber, i.e. a walk-in cold room capable of temperatures down to -30°C. The growth basin was fitted with a pressure relief pipe, which allowed the water to be pushed out of the basin as the ice grew[4]. The basin was divided in two sections: one for the growth of plain ice (no reinforcement), another for the growth of ice with reinforcement. For the latter, before putting water in the basin, the reinforcement material was installed at a desired vertical level across the basin – the set-up is shown in Figure 6.

Water was added into the basin to the desired level, and was brought down to nearly freezing temperature. Its surface was then ‘seeded’, so as to simulate ice growth in nature. This refers to a standard ice growth procedure, whereby water droplets are sprayed into the air (using a source of compressed air that atomizes water) – these fall onto the water surface as tiny ice crystals. This results in a thin layer of slush at the water surface, which grows downward, forming a columnar structure. Such a structure has been traditionally referred to as S2 ice (Michel and Ramseier, 1971), the most common ice type in nature. The ice was allowed to grow to a thickness of about 100 to 120 mm. At that point, the ice was extracted from the basin with an electric chain saw in the form of roughly cut blocks (Figure 7, Figure 8). The full procedure is schematized in Figure 9. All beams were stored at -20°C in an environmental chamber different than the one where ice growth took place, until ready for final beam preparation.

[4] That procedure is a standard practice. The reason it is used is that, when water freezes, the ice occupies a larger volume. Without that system, an increasing amount of pressure would be exerted on the basin walls during ice growth, which could lead to basin collapse. Also the ice cover would be loaded and possible cracks produced.

3.2.2. Ice temperature for testing

The choice of a particular testing temperature was based on considerations related to a real ice cover. On the one hand, the lower surface of floating ice is very close to, or at melting temperature (0°C). On the other hand, the ice becomes progressively colder toward the upper surface of the ice cover, since ambient air in the winter can be much colder, e.g. -10°C or lower. If a snow layer covers the ice, it will afford some measure of insulation. On that basis, an ice temperature close to the freezing point, i.e. between 0°C and -5°C for testing for all tests was deemed to be a good compromise. Although colder temperatures have been shown to induce an increase in the flexural strength of ice (e.g. Gow et al., 1988), this factor is not directly relevant to our investigations, since we are interested in comparing reinforced and non-reinforced ice under the same conditions.

3.2.3. Beam preparation

The day before testing, the rough beams were moved from the environmental chamber where they were stored to the one where the ice was grown. The latter room was set at the target test temperature (-5°C). In order to ensure that all ice specimens had equilibrated to the air temperature, the temperature inside a dummy ice specimen, which always accompanied the beams, was monitored with a temperature probe. It was found that a 24 hour period was sufficient to achieve that equilibrium.

The target dimensions selected for test beams was based on a few factors. The length of the beam was mostly dictated by the size of the equipment and the space available for testing. The choice of a cross-sectional area was based on the range of forces the instrumentation, namely the available load cell, is able to monitor. With these considerations in mind, the target width and thickness was set at 75 mm and 60 mm, respectively. This was achieved by machining the rough beams with a lathe (Figure 10). A set of beams ready for testing is shown in Figure 11 – the beams in that figure are not reinforced.

Recommendations on beam dimensions do exist (Schwarz et al., 1981): beam width should be 1-2 times ice thickness, and beam length should be 7-10 times the thickness. Our target dimensions met the first criterion but not the second one (the ratio was 5), which may have introduced shear effects that impacted flexural strength determination. This does not invalidate the testing outcome, however, since all beams have the same dimensions, and it is the relative strength we are interested in, not the absolute strength. Schwarz et al. (1981) also recommended that the ratio of beam width to ice crystal size must be 10 or higher – this criterion was also met (as seen later).

3.2.4. Reinforcement materials

An overview of investigations on previous ice reinforcement material, and of the factors playing a role in the selection of a candidate material, is presented elsewhere (Barrette et al. , 2019, Charlebois and Barrette, 2019). Three of the materials reported therein were chosen for testing:

- Biaxial Type 2 Geogrid, by Tensar International (Figure 12)
- Stratagrid SG 150, by Strata Systems (Figure 13)
- Standard off-the-shelf ¼ in. (6 mm) threaded rod (Figure 14)

3.2.5. Test set-up

A four-point testing configuration was used for testing (Figure 15). This configuration was preferred over a three-point bending test. The reason is that in a three point bending test, the maximum bending moment occurs directly below the single upper loading point, along a single line. A four-point loading system generates a maximum bending moment along the tensile surface of the specimen that is distributed over the entire zone between the two upper loading points. The aim was to allow fracturing to occur in that zone and to see if any of the flaw structure in the ice acted as a nucleation site for the fracture plane. Either a three-point or a four-point configuration will generate complex loading conditions (Schwarz et al. , 1981). Ideally, a tensional testing arrangement would be the better option to determine ice strength but they are difficult to implement, i.e. far less practical then bending tests.

The load application frame has been used elsewhere (Barrette and Jordaan, 2001) – it is shown in Figure 16 and Figure 17. The load at these points was delivered through a cylindrical rod made of aluminum, with a steel core running along its axis (Figure 18, Figure 19). The aluminum and the steel components may be allowed to slip at their interface. The purpose of this arrangement is to minimize the friction the loading points are exerting on the ice. The loading configuration and dimensions are summarized in Figure 20. The displacement was monitored with a string potentiometer.

3.3. Description of parameters

In this section, we describe parameters of interest for the investigations described in this report. This includes a discussion on what the experimentalist can control, what instrumentation was used to monitor a given parameter and how this information is processed.

3.3.1. Kinematic and kinetic parameters

The parameters involved in this type of research may be divided into two types:

1. *Kinematic*: Parameters that relate to motion or displacement. These include displacement (or strain) rate.
2. *Kinetic*: Parameters that relate to forces (or loads)[5] that cause, or result in, motion or displacement. These include load, strength and work.

Depending on what scenario is being investigated, an experimentalist may use a kinematic or a kinetic parameter for control. For instance, if one is interested in understanding the behavior of an ice cover while *a vehicle is parked on it*, then the controlled parameter will be the load. By applying a constant load on the ice, one would get a time dependent displacement.

The scenario we are investigating in this report is different. It is the time-independent response of the ice cover, i.e. when it is quickly loaded, how much load can it sustain before failing? To do this, displacement rate, not the load, should be the controlled parameter, with a rate that is sufficiently high to simulate this scenario. The test set-up described above was designed for that purpose.

We are assuming that the ice is uniform, homogeneous and behaves in a linear elastic fashion (as explained earlier). Basic concepts in conventional statics mechanics are used (e.g. Gupta, 2013). The resistance in tension and compression on opposite sides of the beam both contribute to the material's flexural strength. Although this is an idealization, these concepts are still widely used in ice engineering.

3.3.2. Displacement and strain

The displacement of the indentor was measured with a Celesco position transducer with a 1270 mm travel (Figure 19). Displacement rate was the speed at which the beam is moving upward against the load cell, indicated in millimeter per second. Strain and strain rate are equivalent to displacement and displacement rate, but are normalized over the initial length.

[5] In this report, 'load' and 'force' are considered synonymous.

3.3.3. Strain

In an idealized elastic behavior, strain ε may be determined as follows:

$$\varepsilon = \frac{6FD}{EWT^2} \qquad \text{Eq. 1}$$

where

- *F* is the load applied at the loading points
- *E* is the elastic modulus
- D, W and T are, respectively, distance between upper and lower support, beam width and beam thickness (Figure 20)

3.3.4. Strain rate

The strain rate is essentially the same thing but it is normalized over the beam dimension. For that reason, it is a unitless number per second. It is derived from:

$$\frac{d\varepsilon}{dt} = \frac{TR}{[LD - (\frac{4}{3})D^2]} \qquad \text{Eq. 2}$$

where

- ε is the strain, $d\varepsilon$ and *dt* are the infinitesimal strain and time increment
- *R* is the speed (displacement rate) at which the indentor moves toward the specimen, in mm per second
- *L* is the distance between the two lower supports

For the N-series, this formula provides a rough strength estimate. For the R-series, it only provides a nominal value, for comparison purposes between the tests. In reality, because the maximum load is achieved after several peak loads, the beam will have changed configuration significantly.

3.3.5. Load

The load, or force, that was applied to the beam was measured by an Eaton load cell with a 1000N capacity, but with a static overload capacity of 150%.

3.3.6. Strength

The standard formula used to determine flexural strength under a four-point loading configuration is

$$\sigma_f = \frac{3FD}{WT^2} \qquad \text{Eq. 3}$$

where

- σ_f is the flexural strength
- *F* is the load applied at the loading points
- D, W and T, as explained earlier (Figure 20)

For the N-series, this formula provides a rough strength estimate. For the R-series, as pointed out above for strain rate, it only provides a nominal value, for comparison purposes between the tests.

3.3.7. Work

Work is a measure of the energy stored in the system, namely in the ice and in the way it accommodates that energy, mainly in the form of elastic distortion and the creation of free surfaces (cracks). Work is determined from

$$W = Fx \qquad \text{Eq. 4}$$

where *x* is the distance traveled by the indentor while it is in contact with the ice surface. The unit for *W* is newton-meter, or joule. This equation is for a scenario where the load is constant. In our tests, the load is not constant but varies with displacement. Computationally, i.e. using the output of the data acquisition system, this can be dealt with by determining each work increment, and performing a summation of all:

$$W \approx \sum_{i=0}^{n} F(x_i^*)\,\Delta x \qquad \text{Eq. 5}$$

where Δx is the displacement increment between each reading, $F(x_i^*)$ is the load at each increment, from the point of contact ($i = 0$) to failure ($i = n$). That equation allows one to address scenarios in which *F* is not necessarily constant, i.e. it can vary during the loading event, which is the case of the testing described in this report. It is the basis for the strain-energy criterion (Beltaos, 1978, Beltaos, 2001), stated as follows:

$$W = \int_S^B F(x)\,dx \qquad \text{Eq. 6}$$

This is the area under a load-time plot. In the above equation, *W* is determined between *S*, the point of load application, and *B,* the point of breakage. The strain-energy criterion is very helpful in quantifying the effectiveness of the reinforcement in being able to resist ultimate failure.

3.4. Testing procedures

All beams were done the same day that the beam was machined to its final dimensions. The width and thickness was measured at both end, so as to obtain an average value (used for strength determination). The beam was then installed on the test frame. The top of the beam was also its upper surface when it was extracted from the growth basin. For the reinforced beams, the distance between the reinforcement and the bottom surface was measured.

To conduct a test, the test frame was lifted upward toward the load cell. Motion speed varied from 0.1 mm to 9 mm/sec. Output from the load cell and from a position transducer was recorded at an interval of 0.002 seconds, i.e. a frequency of 500 Hz, with a 10 Hz filter. A photograph was taken before and after each test; a 4k video clip of each test was also recorded. Representative examples were retained for additional photography and for thin sectioning.

3.5. Test grids and outcome

The test grid for the N-series and the R-series are shown in Table 1 and in Table 2, respectively, along with some of the main results. Data processing was done with MATLAB, a numerical computing software package. Beam response is summarized in Figure 21, Figure 22, Figure 23 and Figure 24. In Table 2, the ice reinforced with threaded rods are treated separately, because the load exceeded the load cell capacity. For these two tests, the load indicated is a minimum.

Table 1: Test grid for N-series. Beam width and thickness uniform to 0.1 mm.

Test	Temp.	L	D	W	T	Displ. rate	Strain rate	Maximum load	Strength (nominal)	Total test time	Total displ.	Work
	deg. C	*m*	*m*	*m*	*m*	*mm/s*	*10^{-3} s^{-1}*	*N*	*kPa*	*sec*	*mm*	*Joule*
N_01	-5	0.300	0.100	0.0755	0.0610	2.5	9.2	1318	1,407	1.000	2.50	1.12
N_02	-5	0.300	0.100	0.0758	0.0613	2.3	8.4	1346	1,417	1.210	2.75	1.10
N_03	-5	0.300	0.100	0.0760	0.0608	2.2	8.1	1367	1,459	1.130	2.50	1.14
N_04	-5	0.300	0.100	0.0750	0.0607	2.2	8.1	1324	1,438	1.130	2.50	1.14
N_05	-5	0.300	0.100	0.0760	0.0590	2.1	7.5	1371	1,554	1.196	2.54	1.08
N_06	-5	0.300	0.100	0.0764	0.0605	2.3	8.3	1619	1,737	1.148	2.63	1.43
N_07	-5	0.300	0.100	0.0640	0.0610	1.4	5.2	1516	1,909	2.070	2.96	1.48
						Minimum		1,318	1,407	1.000	2.50	1.08
						Maximum		1,619	1,909	2.1	2.96	1.48
						Average		1,409	1,560	1.3	2.63	1.21
						Standard deviation		114	192	0.4	0.17	0.17

Table 2: Test grid for R-series. Beam width and thickness uniform to 0.1 mm. The ice with the threaded rods ('Rods') are not considered in the minimum, maximum, average and standard deviation because these tests exceeded the load cell capacity. Minimum, maximum and average values do not include the test results with the rods.

Test	Type	Temp.	L	D	W	T	Displ. rate	Strain rate	Maximum load	Strength (nominal)	Total test time	Total displ.	Work
		deg. C	*m*	*m*	*m*	*m*	*mm/s*	*10^{-3} s^{-1}*	*N*	*kPa*	*sec*	*mm*	*Joule*
R_01	Tensar	-5	0.300	0.100	0.0768	0.0608	2.6	9.6	1517	1,603	5.0	13.17	8.78
R_02	Tensar	-5	0.300	0.100	0.0800	0.0612	1.6	6.0	1550	1,552	5.6	9.21	7.84
R_03	Tensar	-5	0.300	0.100	0.0787	0.0608	4.0	14.7	1848	1,906	3.3	13.13	13.03
R_04	Tensar	-5	0.300	0.100	0.0775	0.0610	2.4	8.6	1381	1,437	2.4	5.75	4.02
R_05	Tensar	-5	0.300	0.100	0.0790	0.0607	2.3	8.2	1376	1,418	2.2	4.96	3.59
R_06	Tensar	-5	0.300	0.100	0.0748	0.0607	2.6	9.4	1570	1,709	4.1	10.46	9.25
R_07	Tensar	-5	0.300	0.100	0.0761	0.0594	2.6	9.2	1385	1,547	3.5	9.08	7.54
R_08	Tensar	-5	0.300	0.100	0.0814	0.0608	2.6	9.6	1339	1,335	3.4	8.96	4.81
R_09	Tensar	-5	0.300	0.100	0.0769	0.0613	2.6	9.6	1516	1,574	4.0	10.46	8.72
R_10	SG	-5	0.300	0.100	0.0718	0.0603	2.6	9.3	1327	1,525	5.3	13.50	8.60
R_11	SG	-5	0.300	0.100	0.0737	0.0608	2.6	9.4	1343	1,479	3.8	9.79	4.86
R_12	Tensar	-5	0.300	0.100	0.0767	0.0603	1.7	6.0	1595	1,716	6.5	10.83	9.40
R_13	Rods	-5	0.300	0.100	0.0833	0.0606	1.3	4.8	2074	2,034	2.8	3.71	3.56
R_14	Rods	-5	0.300	0.100	0.0804	0.0606	1.4	5.0	2074	2,108	3.2	4.38	5.26
							Minimum		1,327	1,335	2.20	4.96	3.59
							Maximum		1,848	1,906	6.5	14	13
							Average		1,479	1,567	4.1	9.9	7.5
							Standard deviation		153	154	1.3	2.7	2.8

3.5.1. 'Failure', 'Breakthrough' and 'Resilience' in the context of beam testing

In the foregoing description of beam testing outcome, we will consider 'failure' to mean the first load peak. For unreinforced ice, it is equivalent to 'breakthrough'. In the case of reinforced ice, several such peaks are observed. They represent resilience to breakthrough.

3.5.2. Load traces plotted against time

In Figure 21, all of the load traces are plotted as a function of time. For the N-series, the maximum load is considered to be equivalent to both the failure load and the breakthrough load. For the R-series, this is uncertain. The following observations can be summarized as follows:

- In all cases, the load and the load rate increases with time up to a peak load.
- For the N-series tests, only one peak is observed in most cases, at which point there is a sudden drop in load and at which point the tests end.

- For the R-series tests, a drop in load also follows the first peak load, but the load climbs again up to another peak in a repetitive fashion, so as to produce a saw tooth pattern, to a significant amount of time.
- The N-series peak loads are relatively consistent.
- In the R-series, deformation up to the first peak load is similar to that of the N-series.
- The Stratagrid material shows comparable initial loads but afterward, the beams did not carry as much load as those reinforced with the other materials. They also show an initial peak load that is higher than all later peak loads.
- The two R-series tests with threaded rods as reinforcement showed the highest resistance, but we are not able to appreciate the load response, since it exceeded load cell capacity. These tests still provide effective guidance, because they indicate this material, or variation thereof, should be considered in the way forward as a good reinforcement candidate.

3.5.3. Effects of displacement rate

In Figure 22, several test parameters of interest are shown (maximum load, total test time to maximum load, displacement to failure, strength and work).

- Maximum load is the highest peak.
- Total test time is the time during which a load was applied before the beam either to fracture in two or pieces (for the unreinforced ice) or the time following the latest peak load, at which point the load progressively decreased (for the reinforced ice).
- Total displacement is that achieved during the test.
- Strength and work are discussed above.

The following observations may be drawn from that figure:

- For the non-reinforced ice, no particular trend is observed, i.e. the displacement rate does not appear to affect the other test parameters, at least within the range of displacement rate used in this test series.
- For the reinforced ice, an increase in displacement rate is associated with an increase in all other parameters. Although the evidence is not strong, due to the data scatter, it is fairly consistent. This trend would have been more obvious had we used a wider range of displacement rates.

3.5.4. Effects of reinforcement location in the beam

In Figure 24, a weak trend may be noticed: the further away the reinforcement was from the bottom surface, the lower the amount of work that was recorded during the test. This is equivalent to saying the closer the reinforcement is to the surface in tension, the more energy was absorbed by the specimen.

3.6. Ice affinity

In order to assess the effectiveness of a reinforcing strategy, a crucial characteristic of the reinforcement material under consideration relates to how well ice grows around or through it. It is important that the reinforcement allows for the ice cover to grow in a manner so to attain its greatest strength. The reinforcing material should be capable of forming some level of bonding with the growing ice. In order to assess whether or not this was the case, a standard thin sectioning procedure was used to examine closely the material inside the ice after beam testing.

3.6.1. Thin sectioning

Thin sectioning procedures were drawn from Sinha (1977), sometimes referred to as the ‘double microtoming technique’. It comprises the following steps:

1) A selected ice specimen is cut with a band saw into an ice slab.
2) The ice slab is mounted on a glass slide, and installed onto a standard microtome device.
3) By shaving off thin layers of the ice, its thickness is brought down to about one millimeter or less.
4) The ice section is then observed either through cross-polarized light, which shows the grain (crystal) structure, or in plain transmitted light, to bring out the inclusions (e.g. air entrapment).

This is a standard observation technique in optical mineralogy. The procedures that were used in the present study are summarized in Figure 25 to Figure 34. It should be noted that thinner ice sections will provide a clearer depiction of the internal structure. For the ice incorporating reinforcement, this could not be done as well as with ice without reinforcement. For the Tensar geogrid, the ice was a little thicker but nonetheless provided the required information. The ice enclosing the Stratagrid and the threaded rods was not observed.

3.6.2. Thin section observations

The outcome of thin section observations may be summarized as follows:

- The reinforcement material got incorporated into the ice structure seemingly without significantly affecting the ice structure.
- The reinforcement material, however, appears to have been a nucleation site for air bubbles (Figure 36). This was observed in the water prior to freeze-up.
- There is clear evidence that beam breakage is affected by the presence of the reinforcement material, as indicated by a cleavage of the ice after failure. Evidence of that cleavage is shown in Figure 36.

3.7. Discussion

The outcome of the beam testing program reported herein and in our earlier report (Barrette et al. , 2019), provides helpful information on the response of ice-strengthened beams subjected to a flexural loading regime. Following are some conclusion that may be drawn on the various experimental outcome.

3.7.1. Ice affinity

Ice is notorious for not accepting anything inside its structure. This is why the air contained in water does not get incorporated inside the crystal lattice, and instead accumulates at grain boundaries in the form of air bubbles. Although the incorporation of a solid membrane into the ice is a different scenario altogether, it is an important question because if the presence of the ice-membrane interface creates a weakness plane, this could conceivably defeat the purpose of ice reinforcement. The observations summarized above provide evidence that the crystal structure makes its way around the material (Figure 35, Figure 36, Figure 37, Figure 38). In a purely extensional loading regime, this would be desirable, because the crystals around the material would be expected to keep taking up the load. However, in a flexural loading regime, shear action is expected to occur. In that case, any new interface (such as that between the reinforcement material and the ice) would likely promote sliding along it. This is what appears to have happened, as shown by the cleavage cracks in Figure 36.

Observations of the interface between the threaded rods and the ice were not obtained. The irregular nature of the rods (i.e. the threads) likely prevented, at least to some extent, slippage at this interface. It is not known how much that could have played a role in making that material more effective (than the others) in strengthening the ice. If it did, however, it would have mobilized the elastic modulus of the metal, which is considerably higher than that of the ice. Without further evidence, that is an assumption that can be made at this time.

3.7.2. Resistance to ice failure

For the ice beams without reinforcement, there is only one peak, after which load resistance vanishes. For the reinforced beams, several successive peaks are seen, generally with a progression in the height of the peak (except for the two Stratagrid-reinforced beams). The highest peak is used as the maximum load for these tests. Because the beams reinforced with threaded rods show the highest resistance, and the least displacement at failure, this points to rods, or something similar, as an appealing option to reinforce ice. No clear difference in strength is documented between the two geogrids (Tensar and Stratagrid).

It can be assumed that the sudden drop following most peak loads is concurrent with the generation of one or more fracture planes. This, however, cannot be unequivocally demonstrated because the video sequences were not synchronized with the data acquisition.

The existence of the cleavage at the interface between the ice and the reinforcement material may conceivably weaken the ice. However, that cleavage was also observed in the ice reinforced with the threaded rods, which showed a high resistance to failure.

3.7.3. Effects of strain rate

That the strain rate affects beam resistance to failure (i.e. maximum load) for R-series, but not for N-series, is an interesting observation (Figure 23). This is likely due to time-dependent deformation mechanisms, i.e. the development of fractures, whose contribution to beam response is larger at a lower strain rate.

3.7.4. Resilience

The reinforced ice beams show a higher resistance to breakthrough (resilience, as defined in section 1.5.2) than the non-reinforced ones. This is shown by the work exerted on these test specimens, which is considerably higher than that on the non-reinforced beams. The trends shown in Figure 23 all express the response of these beams, as shown in Figure 21, i.e. the longer it takes for the load to vanish, the more energy is expended by the system (and absorbed by the ice). This indicates that, despite the fact the material did not increase resistance to failure, it did contribute to an increase in resilience, which translates into a higher resistance to breakthrough.

As for the non-reinforced beams, work is independent of the other parameters. All average around 1 joule, significantly lower than the reinforced beams.

3.7.5. Effects of reinforcement location in the beam

The trends shown in Figure 24 are compatible with the expected load response. The closer the material is to the lower surface of the beam, the more effective it will be to prevent beam failure and breakthrough. It points to the importance of placing the reinforcement as close as possible to the anticipated bottom surface of the ice. If deployment is before water freeze-up, then the material should be installed at a water depth as close as possible to the expected freezing front. If deployment is after freeze-up, for instance by inserting the material through a slot in the ice, that procedure should be conducted just before the ice has achieved its maximum thickness (upon further growth, the ice would then enclose the material).

4. Second phase: Plate testing

So far, we have described the outcome of testing on ice beams, i.e. relatively small, prismatic ice specimens. The second phase of this project is a step closer to a real scenario. This was done with larger, plate-like ice specimens, more akin to a real 3D representation.

4.1. Objectives

The objectives of the second phase are similar to those in the first phase (section 3.1): to assess the difference in ice behavior between non-reinforced and reinforced ice. This will be done into two stages:

1. A preliminary stage, the outcome of which is *in this report*, where procedures will have been devised and implemented, and some basic analyses of test outcome will lead the way to the follow-up stage;
2. A follow-up stage, where the procedures will have been fine-tuned, the outcome of which will be included *in next year's report*.

4.2. Rationale

Information on ice response due to loading can be investigated in various ways. As mentioned above, beam testing in a laboratory is a simple and very elementary approach to gaining insights into these scenarios. As for plate testing, there are various degrees as to how closely it can approach the target scenario. For the present investigations, we chose to focus on the salient aspects of the event, e.g. ice thickness and properties, reinforcement properties and boundary conditions. The ice plates were not floating, such that buoyancy was not factored in. Also, in floating ice, there is a temperature variation across the ice thickness (0°C at the ice water interface). That factor was not captured either.

Hence, although the second phase described here is seen as a step closer to a real scenario, it is still relatively distant from it. Nonetheless, it is a logical step in progression, and is expected to lead the way to more complex testing. Furthermore, the fundamental basis of the work presented herein was to compare non-reinforced and reinforced ice. Thus, it is not the absolute parameter values that are sought in these investigations, as much as a difference in response, both qualitative and quantitative.

4.3. Challenges

While beam testing (Phase 1) relied on relatively common procedures, plate testing is unusual. As is often the case in novel test set-ups and accompanying procedures, some dilemmas and challenges had to be overcome. They included the following:

- The ice plate had to be thick enough (at least 100 mm) to allow incorporation of the reinforcement material. The equipment and instrumentation had to take into account the amount of vertical load and displacement required to achieve complete breakthrough.
- Ice growth to a sufficient thickness requires time – up to several days. To achieve a reasonable number of tests within an acceptable time frame, we had to think about doing more than one test, perhaps several, for each growth episode.
- The wider the ice plate, the closer to full-scale behavior. However, this also means the lesser the number of tests that could be done with the available resources.
- Appropriate loading frames were required, capable of withstanding the amount of vertical load required to break the ice plates.
- These frames would be built and assembled outside the cold room where the tests would be conducted. As such, their size could not exceed the size of the room's door.
- Incorporation of the reinforcement material into the ice would follow a similar scheme as for the first testing phase (section 3.2.1, Figure 6). But the material would have to be reasonably planar and horizontal – the larger the frame size, the less achievable that becomes.
- Regardless of the chosen test set-up, the seeding technique described earlier in this report (section 3.2.1) was to be used, so as to produce standard ice. Once the ice had grown to the

target thickness, a procedure had to be devised to load that ice vertically, so as to obtain information on its flexural behavior.
- A means of applying the vertical load at the desired location on the ice surface was required.

4.4. NRC's ice tank facility

The NRC's ice tank in Ottawa is a pool-size basin inside a refrigerated chamber that simulates Arctic and northern marine conditions. It is a versatile facility that has been used in the past number of decades to study a large number of ice-related scenarios. The tank itself, made from concrete, is 21 m in length, 7 m in width and 1.1 m in depth. It is equipped with a carriage, which is a structure spanning the full width of the tank, traveling on rails, and used for towing or for carrying instrumentation and actuators. The temperature inside the chamber can be varied down to -20 °C and can produce ice of up to 0.6 m thick.

4.5. General overview

All tests were done in the ice tank. A four-step procedure was adopted (Figure 39). The following is a quick overall summary of the procedures used to overcome the aforementioned challenges:

- Testing on an ice sheet (grown inside the tank) was the preferred option because it allowed several tests to be done for each growth episode – the latter requiring a full week to achieve the desired ice thickness. This option contrasts with an alternative considered earlier, which would have been to do one test per growth in a much smaller test basin.
- A diameter of 2.5 m for each frame was chosen as a compromise between size and number of tests. This was also the maximum size that could fit through the chamber's door.
- Eight load frames of that size could fit in the ice tank – these frames were custom-made by a local manufacturer and delivered to NRC's location in Ottawa.
- The frames were deployed into the ice tank, as shown in Figure 40.
- They were anchored and leveled (Figure 41), and some lights were installed below some frames (W2, W3, W4), for later visualization of cracking pattern in the ice.
- The reinforcement materials were installed, using nylon cables anchored to the tank's walls (Figure 42).
- The tank was filled with water (Figure 43), the temperature was lowered so as to be able to form an ice cover after seeding (Figure 44, Figure 45). The top of the load frames was always well below the freezing front.
- The ice above (and around) each load frame was cut (Figure 46) and the water level was lowered so as to bring the ice resting onto the load frame below (Figure 47).
- For each test, the ice tank carriage was then moved above the plate to be tested (Figure 48).
- A piston was mounted on the ice tank carriage, and used to apply the vertical load (Figure 49) while the instrumentation recorded ice response (Figure 50, Figure 51). All connections were on the carriage.
- The displacement sensors were mounted on a horizontal bar, and an acoustic sensor was frozen onto the ice surface (Figure 51).
- Figure 52 shows an example of test outcome – the cracked surface of an ice plate at the end of a test.

Additional information is provided below.

4.6. Details of the methodology

4.6.1. The test frames

The eight test (or load) frames were built by a contractor using standard steel flat bars 127 mm in width and 12.7 mm in thickness, welded into circular hoop with a target diameter of 2.5 meters. The frames were not perfectly circular – final external dimensions ranged from 2.48 m to 2.54 m. They were positioned inside

the ice tank. All frames were mounted on three steel legs and leveled prior to anchoring using shims and a plum line. The top of the frames was at a height of approximately 770 mm above the tank floor. A light source was installed below a few frames (W2, W3, W4), for later visualization of cracking pattern in the ice.

4.6.2. Reinforcement

Type

The choice of materials that would be used for reinforcement was based on the outcome of the Phase 1 testing, as well as on an earlier inquiry (Barrette et al. , 2019):

- Triaxial TX7 geogrid, from Tensar International (Figure 53)
- Steel cables (Figure 53): These were chosen as the nearest practical equivalent to threaded rods (used during the beam testing phase). Two cable diameters were used: 3.2 mm and 6.4 mm. In addition, we varied the number of strands (4, 7 and 10 strands). The layout is shown in Figure 54.

Mounting

Once a decision had been made about what the type of reinforcement would be used for each test frame, a system was devised to extend them inside the ice tank above each frame. This was done as follows (Figure 55, Figure 56, Figure 57, Figure 58):

- Two sets of sleeved steel lines, oriented in an E-W (across the ice tank's width) and N-S directions (across the ice tank's length), were anchored on the ice tank walls.
- The steel cables were tied to wooden bars, which were themselves were attached to the lines with plastic cables.

This system's purpose was to have the reinforcement relatively leveled and within a flat surface. This was achieved to a large extent.

4.6.3. Ice plate production

A three-step procedure was adopted – these steps were:

1) To grow the ice down to sufficient depth (about 120 mm) until it enclosed the reinforcement material.
2) To cut the ice around each load frame into individual plates.
3) To partially drain the ice tank, thereby lowering the plates so that they came to rest on top of the load frames below.

More details about this procedure are now provided.

Ice growth

Ice growth followed a standard ice tank practice:

- The ice tank was filled with water to the target level, and that water was allowed to cool down to freezing temperature. This was done by lowering the air temperature to -15°C. That cool-down period required seven days (Table 4). Once a thin layer of ice had begun to form at the water surface, it was carefully removed with a screen attached to the carriage. Precautions were taken to keep the screen from hitting the frames below the water surface during carriage travel.
- Immediately after that ice was removed, seeding proceeded. This was done by connecting an air supply feeding from a small jug filled with water. A special nozzle allowed projection of a tiny mist into the air, which froze and settled onto the water surface, thereby creating a uniform layer of slush 1-2 cm in thickness. That seeding process was done within one hour.
- Downward growth of the ice took place during 5 days, leading to a maximum thickness of up to 130 mm. As may be seen in Figure 59, ice thickness was not uniform across the length of the ice tank, i.e. an increase of up to 20-25 mm was observed toward the south, and a similar increase toward the west. This has to do with air circulation inside the ice tank. On average, growth rate was about 1 mm/hour. The ice thickness was measured and accounted for in the analyses.

Internal structure of the ice

The outcome of the seeding procedures leads to the formation of columnar-grained ice, an example of which is shown in Figure 34[6]. Thin sections from the ice in the ice tank were not made to confirm this assumption, as numerous previous ice tank tests can confirm[7].

Incorporation of reinforcement into the ice

Both the polypropylene geogrid and the steel cables were incorporated into the ice with relative success, but neither were perfectly flat. For some tests, the cable segments did not get incorporated (Figure 60) – information in that regard is included in Table 5. As explained later, this is attributed to ice melting due to a failure in the refrigeration system. During ice growth, air entrapment formed preferentially at the ice-material interface (Figure 61) and, in the case of the steel cable, air entrapment lined up in the ice column above it (Figure 62).

Ice plate production

An electric chainsaw was used to cut around each of the load frames. It was able to cut through the ice and the plastic cables used to anchor the reinforcement to the tank walls. The water inside the tank was then drained to well below the top of the load frames, allowing each ice plate to come down and rest directly on the frame below.

4.6.4. Instrumentation

The instrumentation included:

- An actuator, consisting of a hydraulic piston and a 4.5 kN capacity load. The actuator, which also incorporated a transducer to monitor displacement, was used to apply the load onto the ice at a desired displacement rate.
- Six spring-loaded linear variable inductance transducers (LVIT), with a 0-50 mm range and a 0-10 VDC output. These were used to monitor ice deflection.
- An acoustic emission system, consisting of a two-channel system and one sensor. This system was used to monitor cracking activity.
- A temperature profiler, consisting of 13 thermistors mounted on a plastic rod and spaced at a 10-mm interval (Figure 63). It was used to monitor the temperature of the water, the ice and air, at a given location in the ice tank. That location was away from all tests.

Prior to testing on ice, a trial run was done on wood at room temperature as a test for the instrumentation. A wood beam (a standard '2-by-4') was used for that purpose. It spanned the full diameter of a frame. The load was applied onto it while the transducers recorded displacements.

4.6.1. Load application

Two options for load application were considered early in project planning, i.e. either:

1. To move the actuator at a constant displacement rate. This is referred to as displacement-controlled, in the sense that the controlled parameter is actuator position. The main advantage of this option is simplicity of the system required to achieve this loading mode.
2. To move the actuator until it contacted the ice, then ask the system to maintain a constant load. This is referred to as load-controlled, in the sense that the controlled parameter is the load. The advantage of this approach is that it can provide information on the time-dependent behavior of the ice, i.e. the plate response as a function of time.

Option 1 was retained for this test program. More information on the theory of ice response may be found elsewhere (Barrette, 2015).

The load was applied onto the ice plates via a circular stainless steel platen 100 mm in diameter and 10 mm in thickness Figure 64. A 5-mm thick foam pad was put onto the ice at the loading point, so as to avoid localized stresses.

[6] That ice is often referred to as 'clear' ice in natural ice covers. It is quite different from the white ice produced via flooding procedures, which is made from equiaxial grains, with a substantial amount of air entrapment (which is why the ice looks white).
[7] A strong indication was the tendency for air entrapments in the ice to line up vertically (they normally do so along grain boundaries).

Information on the eight plates that were tested is shown in Table 3. It includes initial plate thickness and the actual thickness of the plates as tested. The difference between these two data is due to failure of the refrigeration system, which caused the air temperature to increase above melting point – this is explained later. For all tests, the displacement rate was 1.4 mm per second, with load duration varying from about 20 seconds to 77 seconds, depending on plate response (Table 3). This rate was chosen so as to allow visual appreciation of the plates' deformation response, which was recorded on video.

Table 3: Information on the plates. Initial plate thickness is that prior to warm-up episodes discussed later. Data for W1 were not collected due to an error in procedures. Light blue cells are for non-reinforced ice; light green cells are for plates reinforced with the geogrid; light grey cells are for plates reinforced with steel cables.

Test	E1	E2	E3	E4	W1	W2	W3	W4
Initial plate thickness (mm)	110	110	100	95	125	127	120	109
Thickness of tested plate (mm)	64	71	53	79	125	127	120	109
Duration (seconds)	22	43	22	46	N/A	77	77	67
Number of radial cracks	21	18	20	8	8	14	11	11

In some cases (tests E1 and W2), platen displacement rate was not rigorously constant. In these cases, a short but abrupt deviation in load occurred. The reason for these glitches is uncertain. It may have to do with the ability of the piston to adjust to ice response – during sudden load drops, it may not have been able to do so.

4.6.2. Acoustic Emission Testing

Acoustic emission testing (AET) is key to understanding crack formation. This has been implemented on engineered material such as metals, asphalt and concrete (e.g. Sinha, 1996, Soulioti et al., 2009). It has also been used on ice in experimental set-ups, namely by NRC researchers (Gold, 1960, Sinha, 1985) and others (e.g. St. Lawrence and Cole, 1982, Li and Du, 2016). A few studies have also been done in the field (Langhorne and Haskell, 1996, Lishman et al., 2019). Information was thereby generated on stress-induced cracking activity, the effects of temperature, and source location.

AET has never been used on ice in our OCRE Ottawa facility. This project was an opportunity to explore this technique and how it can be applied to ice response.

General principle

AET is a type of non-destructive monitoring technique applied to a large number of engineering scenarios. The basic principle is that a crack emits an elastic wave that travels through the ice (Figure 65). An AE sensor is able to detect that activity (Figure 66). It contains a piezoelectric crystal, which upon recording the pressure associated with such a wave[8], generates an electric signal. Hence, when a crack forms, two things happen (Figure 67):

1) A permanent change inside the material, i.e. the existence of an additional crack,
2) A wave travels in all directions – it is a short-lived (e.g. microseconds) pulse-like event, characterized by a duration and an amplitude.

A simplified diagram of an AE event is shown in Figure 68, where the voltage generated by the sensor is plotted against time:

[8] The stress is the outcome of an inertial acceleration and related force on the sensor's internal components.

- *Threshold*: Minimum voltage required to be considered a significant event, e.g. above background noise.
- *Rise time*: Time required to reach maximum amplitude.
- *Counts*: A single event may have several counts, which are voltage peaks exceeding the threshold limit.
- *Duration*: The time window that includes all counts – it may be in the order of microseconds.
- *MARSE*: The area that includes all counts, including below the threshold.

For the purpose of this report, only the counts were be monitored, as a preliminary step toward a more comprehensive procedure.

The sensor used in this study is shown frozen onto the ice (with a small amount of water) in Figure 69. It is a wideband frequency sensor, with an operating frequency range of 200-850 kHz.

Following are some of the characteristics of AET, which should help to outline the potential and limitations of this technique for both laboratory and field deployment:

- In general, AET is a passive technique – the sensor does not generate any energy; it only listens.
- It can allow a full volumetric inspection of a given structure if several sensors are used.
- The system does not require maintenance – the sensor can remain in place throughout a structure's operational lifespan, provided it is robust enough to sustain the environmental conditions.
- The output can be recorded remotely.
- It provides a qualitative assessment of the material response, albeit not a quantitative description of the material's state. The latter requires other tools – in the case of ice, it could be core sampling and thin sectioning.
- Another limitation is that it may not work well in a 'noisy' environment, i.e. one in which there is sound generated by other sources, which have nothing to do with the ice response, for instance, wind action on the ice surface or someone walking next to the sensor(s).

4.7. Time frame for testing

The time frame over which the bulk of Phase 2's first stage was achieved is listed in Table 4. It spanned about five weeks.

Table 4: Time frame over which stage 1 of Phase 2 testing was accomplished (2019). This does not include the time to prepare for testing, e.g. planning, frame construction, instrumentation procurement and development.

Date	Business day	Activity
Tuesday, July 16	1	Delivery of test frames to M32
Tuesday, July 23	6	Completion of frame mounting in ice tank
Wednesday, July 24	7	Testing and validation of instruments (a piece of wood was used in lieu of ice)
Thursday, July 25	8	Water in tank, bringing the temperature down to -15°C
Seven (7) calendar days		
Thursday, August 1	12	Seeding: initiation of ice growth
Five (5) calendar days		
Tuesday, August 6	15	Target ice thickness achieved
Wednesday, August 7	16	Chain sawing operation completed
Monday, August 12	19	First test completed
Friday, August 16	23	Transport Canada and CIRNAC witnessed a test (E4)
Wednesday, August 21	26	Last test completed (E1)

4.8. Test grid and boundary conditions

The test grid for plate testing is shown in Table 5. A total of eight plates were tested – for each, as shown in that table, information is provided on reinforcement, the ice thickness as well as on the boundary conditions. These refer to the interaction between the test frames and the ice.

Due to a technical difficulty, testing did not proceed as planned. After the first three tests were conducted (W1 to W3), the refrigeration system failed, allowing the room temperature to climb above 0°C. This caused ice to melt, the extent of which is uncertain. The system was fixed, but underwent another major failure again after test E4, i.e. before testing on E3. The ice structure was not expected to change due to these melting events. However, that is undoubtedly why some of the steel cables ended up not being fully enclosed in the ice before testing (recall that the cables were not rigorously horizontal). It is also suspected that the temperature prior to W4 was also affected, but only to a small extent.

Furthermore, as a results of these failures, the last five tests (W4, E4 to E1) have been done under different boundary conditions (Figure 70). As shown in Figure 70b, two types of infinitesimal motion were possible during these tests:

- A rotational component, i.e. whether or not the plate was allowed to rotate about a horizontal hinge along the ice/frame interface.
- A lateral component, i.e. whether or not the plate was allowed to move sideways.

The warm-up events caused the load frames to either freeze onto the ice and/or to penetrate a certain distance into the ice plate (see information provided in Table 5 on parameters A and B, Figure 70). Hence, for test W1 to W3, both R and L were allowed. For test W4, we suspect R was allowed but not L. For the tests E4 to E1, neither were allowed. It is also conceivable that adfreeze (i.e. freeze-up of the ice onto the frame) occurred, regardless of the warm-up episodes. This will be addressed in future testing.

Table 5: Tests grid - location is shown in Figure 40. 'A' in the third column, and 'B' in the 'Comments' column, are that indicated in Figure 70. Boundary conditions (BC) are shown in the 5th column: N: no rotation allowed, R: rotation allowed, L: lateral motion allowed.

Test	Reinforcement	Ice thickness above frame A (mm)	Average depth of reinforcement below the ice surface (+/- 20 mm)	BC	Comments
E1	None	64	No reinforcement	N	Because of the two melting episodes mentioned earlier, before testing, the load frame had melted its way into the ice about 60 mm (B).
E2	Geogrid TX7	71	70	N	The ice in this test suffered the two melting events mentioned earlier, before being tested. The reinforcement was either very close to the frame or right against it. Also, the load frame melted its way into the ice about 50 mm (B).
E3	Steel cables 3.2 mm, 7 strands	53	50	N	A second warm-up incident occurred before this test. The reinforcement was either very close to the frame or right against it. The ice became thinner and the load frame melted its way into the ice about 35 mm (B). The cables may have been only partly enclosed in the ice – that verification was overlooked.
E4	Steel cables 6.4 mm, 4 strands	79	80	N	Most of the cables were below the ice plate or just at the interface. Because of a melting episode prior to that test (the second one), the ice became thinner and the load frame melted its way into the ice about 20 mm (B). The cables were only partly enclosed in the ice.
W1	None	125	No reinforcement	R,L	No data were collected during this test, due to an error in the test procedures (the length of test preparation was underestimated).
W2	Geogrid TX7	127	80	R,L	The full grid surface was fully enclosed.
W3	Steel cables 3.2 mm, 7 strands	120	90	R,L	All cables fully enclosed.
W4	Steel cables 6.4 mm, 10 strands	109	110	R	Over 75% of cable out of the ice, i.e. all were mostly out, except two. The ice for this test may have been affected by a temporary increase in temperature although it was not severe enough to cause the frame to penetrate into the ice (B=0). However, it is suspected that unlike for tests W1, W2 and W3, the ice may have been 'welded' onto the frame.

4.9. Testing outcome

The outcome of all instruments is summarized in Appendix B – Plate deflection in response to loading, and in Appendix C – Acoustic sensor response in response to loading.

4.9.1. Visual observations

The following visual observations were made on plate response during each of the test:

- The most noticeable difference in behavior between non-reinforced and reinforced ice is the time that was required for plate failure. In test W1 (non-reinforced), the plate collapsed within 1-2 seconds after load application. It did so via the formation of eight radial cracks at about 45 degrees intervals. Immediately afterward, all slices physically collapsed down at once under their own weight.
- The other test on non-reinforced ice (E1) failed in a progressive manner, like the other reinforced ice tests. This points to the role of the boundary conditions (the plate was not able to rotate at the hinge). Considerable resistance to failure was afforded along the ice/frame interface, indicated by the development of cracks at that location. The gravity collapse seen in W1 did not occur in E1. Instead, the platen punched a hole into the ice plate.
- In all tests with reinforced ice, a series of radial cracks developed within several seconds of load application, as was the case for both tests with non-reinforced ice (E1 and W1). This was followed by the continued development of crack networks. In none of these tests did the ice fall down under its own weight, as it did for W1.
- The final number of radial cracks - cracks that extend from the platen to the plate's perimeter – is indicated in Table 3. The cracks were vertical and spanned the plates' full thickness.
- There were two sources of secondary cracking activity, i.e. that occurring after the initial radial cracks: either the radial cracks themselves, or the ice/frame interface. In the latter case, the cracks migrated from the ice/frame interface toward the center.

4.9.2. Deflection in response to loading

The following information was obtained from the instrument response:

- In all cases, piston/platen motion proceeded at a steady pace, with one exception (test W2), where the piston came back up slightly then resumed its downward motion. This is attributed to the piston response to sudden ice failure – it may not have been able to adjust properly.
- In all cases, the load response shows a saw-tooth pattern, each peak being preceded with a load increase, and followed by a sudden drop.
- Boundary conditions that did not allow plate rotation at these boundaries led to higher loads (above 10 kN), especially for E1 and E2. The maximum load for the other tests were below 10 kN.
- Tests W2 and W3 are the only two tests done with boundary conditions in rotational mode at the hinge, and that were not affected by the failure of the ice tank's refrigeration system. The loads recorded for test W2 (with the geogrid) are considerably higher than those for test W3. This cannot be accounted by the small difference in ice thickness (Table 5). Additional analyses and further testing are required to confirm that observation.

Because no data were collected for W1, a proper appreciation of the difference between non-reinforced and reinforced ice cannot be made.

4.9.3. Acoustic sensor response

For the purpose of the present project phase, our analysis of AET outcome is exploratory. We focus on one parameter: peak counts (Figure 68). The AE sensor collects information from crack sources distributed throughout the entire plate.

The following observations can be made:

- As can be seen from all plots in Appendix C, there is some correspondence between the overall AE activity and load cell response. The higher drops in loads are often accompanied with a

reduction in AE activity. A more detailed analysis would be required to further investigate the correlation of load fluctuations and AE activity.

- In general, the amount of AE activity is higher at the beginning of the test, even before the maximum load is achieved. The two exceptions were E3 and E4, which showed intense activity throughout the tests. This could have been caused by the action of the free cable spans below the ice.
- Despite the lower loads recorded during W3 (cables) compared to W2 (geogrid), AE activity is higher in the former than it is in the latter.
- AE activity could be roughly divided into 1) continuous, where there are no drops in counts, and 2) intermittent, where the drops fall to nearly zero. Gradients between these two behaviors are also observed.

5. Summary and way forward

5.1. Beam testing

In this report, the outcome of the final phase of beam testing is reported. The following may be derived from that phase:

- Reinforcement does not always increase the resistance to failure (first crack). It did so with the threaded rods, but with the two geogrids there is no clear evidence of this. This observation favors using steel cables as the nearest practical equivalent for reinforcement of an ice cover.
- Geogrids, especially Tensar, are effective at absorbing the energy delivered onto the ice by a vertical load. This material could be envisaged for further investigations.
- The ability of the ice to grow through the material is an important aspect of ice reinforcement. It has been shown that ice crystals do make their way around it for the geogrid.
- However, the ice/material interface can introduce a plane of slippage, which is suspected to act as a weakening factor. One option is to investigate a 3D geogrid, such as a geocell, to reduce shear.
- The closer the reinforcement is to the bottom of the beam, the higher the resistance to loading.

5.2. Plate testing

A preliminary series of plate tests was conducted. Its purpose was to design and implement a procedure to carry out plate testing, and to generate preliminary data on plate response. Steel cables and a geogrid were selected as ice reinforcement materials.

The following may be derived from the test series documented in this report:

- A procedure for incorporating these materials into the ice and to produce large ice plates for testing was successfully implemented.
- All instrumentation – load, displacements and AE – performed satisfactorily.
- A consistent plate bending response was recorded at the very beginning of the loading event, yielding important information for the validation of numerical models.
- A clear correlation was established between load cell response and AE.
- Technical difficulties had an impact on data quality/output:
    - Instrumentation output for one test on non-reinforced ice was not collected.
    - Failures of the refrigeration system introduced a new test parameter to be considered in the analyses: boundary conditions and their effect on plate response.
    - Actuator/piston motion was not linear in one test.

5.3. Way forward

The work accomplished to date opens the way to the second series of plate testing. A number of aspects could be addressed. These are listed here.

<u>Short-term loading response</u>

This is the elastic response of the ice leading to its initial failure, i.e. the first set of cracks. Deflection profiles across the ice sheet are shown in Appendix B, for three different times after loading. This response should be analyzed, using normalized or dimensionless parameters, such as stress and displacement to ice thickness ratio. The role of reinforcement in increasing the elasticity modulus of the ice should be evaluated.

<u>Correspondence between visual and instruments</u>

A better understanding of the plate response could be gained by comparing the visual information on the video sequence of each test and the instrumentation output for that test. Does all cracking activity lead to load drops? What are the extent and location of the cracks responsible for the most important load peaks and AE activity? Can reinforcement reduce cracking activity, or even induce it?

AE response – further analyses

Elastic wave energy in deforming ice can be examined in a number of ways – this can generate instructive insights on ice response with and without reinforcement. What is presented in this report is exploratory – it could be followed up with additional analyses.

Numerical modeling

Numerical modeling of the ice behavior in the elastic domain could be validated against the outcome of the plate test series. The ultimate purpose of this endeavor would be to assess the capability of this tool to foresee ice failure of non-reinforced and reinforced ice. Its ultimate aim is to develop a predictive tool for field scenarios.

Preliminary assessment of field deployment

This task would include material certification and an investigation of further deployment options. The choice of reinforcement would also be discussed further. For instance, the use of a 'geocell' could address the shearing component inside the ice during vertical loading (Gold, 1990). Material availability, density (whether if floats or not), ease of transportation (rolls, weight) are aspects that could be looked into further.

6. Acknowledgements

The work reported herein is part of a multi-year project spanning three fiscal years (FY2018-19, FY2019-20 and FY2020-21). It is financed by Transport Canada's Northern Transportation Adaptation Initiative (NTAI) Program, Crown-Indigenous Relations and Northern Affairs Canada (CIRNAC) and NRC's Arctic Program. Beam testing was done with Bradley Butt's assistance in St. John's. Plate testing was done in Ottawa with the assistance of David Hnatiw, Yvan Brunet, John Marquardt and Tony Frade. This report benefited from comments by Bob Frederking, Hossein Babaei, Denise Sudom and Anne Barker.

7. References

Barrette, P., Charlebois, L. and Butt, B., 2019. *Reinforcement of ice covers for transportation: Material investigation and preliminary laboratory testing*. OCRE-TR-2018-031. National Research Council. Ottawa.

Barrette, P.D., 2015. *Overview of ice roads in Canada: Design, usage and climate change mitigation*. OCRE-TR-2015-011. National Research Council of Canada. Ottawa.

Barrette, P.D. and Jordaan, I.J., 2001. *Beam Bending and Fracture Behaviour of Iceberg Ice*. 4-78.

Beltaos, S., 1978. *A strain energy criterion for failure of floating ice sheets*. Canadian Journal of Civil Engineering, 5, p. 352-361.

Beltaos, S., 2001. *Bearing capacity of floating ice covers: Theory versus fact*, 11th Workshop on the Hydraulics of Ice Covered Rivers. Committee on River Ice Processes and the Environment (CRIPE), Ottawa, Canada.

Charlebois, L. and Barrette, P., 2019. *Ice reinforcement: Selection criteria for winter road applications and outcomes of preliminary testing*, Proceedings of the 18th International Conference on Cold Regions Engineering and of the 8th Canadian Permafrost Conference, Quebec City, pp. 119-127.

Gold, L.W., 1960. *The cracking activity in ice during creep*. Canadian Journal of Physics, 38(9), p. 1137-1148.

Gold, L.W., 1990. *The Canadian Habbakuk Project*. International Glaciological Society 1993, 323 p.

Gold, L.W., 2004. *Building ships from ice: Habbakuk and after*. Interdisciplinary Science Reviews, 29(4), p. 373-384.

Government of the NWT, 2015. *Guidelines for safe ice construction*. Department of Transportation, Yellowknife, Canada, pp. 44.

Gow, A.J., Ueda, H.T., Govoni, J.W. and Kalafut, J., 1988. *Temperature and structure dependence of the flexural strength and modulus of freshwater model ice*. Cold Regions Research & Engineering (CRREL). New Hampshire.

Gupta, V., 2013. *Theory of pure elastic bending*.

Hori, Y. and Gough, W.A., 2018. *The state of Canadian winter roads south of the 60th parallel: historical climate analysis and projected future changes based on the climate model projections*. University of Toronto. Toronto.

Hori, Y., Gough, W.A., Butler, K. and Tsuji, L.J.S., 2017. *Trends in the seasonal length and opening dates of a winter road in the western James Bay region, Ontario, Canada*. Theoretical and Applied Climatology, 129, p. 1309-1320.

Langhorne, P.J. and Haskell, T.G., 1996. *Acoustic emission during fatigue experiments on first year sea ice*. Cold Regions Science and Technology, 24, p. 237-250.

Li, D. and Du, F., 2016. *Monitoring and evaluating the failure behavior of ice structure using the acoustic emission technique*. Cold Regions Science and Technology, 129, p. 51-59.

Lishman, B., Marchenko, A., Shortt, M. and Sammonds, P.R., 2019. *Acoustic emissions as a measure of damage in ice*, Proceedings of the 25th International Conference on Port and Ocean Engineering under Arctic Conditions (POAC), Delft, The Netherlands.

Michel, B. and Ramseier, R., 1971. *Classification of river and lake ice*. Canadian Geotechnical Journal, 8(1), p. 38-45.

RSI, 2014. *Tibbitt to Contwoyto Mining Road - Historical climate analysis*. Ottawa.

Schwarz, J., Frederking, R., Gavrillo, V., Petrov, I.G., Hirayama, K.-I., Mellor, M., Tryde, P. and Vaudrey, K.D., 1981. *Standardized testing methods for measuring mechanical properties of ice*. Cold Regions Science and Technology, 4, p. 245-253.

Sinha, N.K., 1977. *Technique for studying structure of sea ice*. Journal of Glaciology, 18, p. 315-323.

Sinha, N.K., 1985. *Acoustic emission study on multi-year sea ice in an Arctic field laboratory*. Journal of Acoustic Emission, 4(2/3), p. S290-S293.

Sinha, N.K., 1996. *Acoustic emissions in asphalt subjected to thermal cycling at low temperature*, Proceedings of the 6th Conference on Acoustic Emission/Microseismic Activity in Geologic Structures and Materials, Zellerfield, pp. 109-120.

Soulioti, D., Barkoula, N.M., Paipetis, A., Matikas, T.E., Shiotani, T. and Aggelis, D.G., 2009. *Acoustic emission behavior of steel fibre reinforced concrete under bending*. Construction and Building Materials, 23, p. 3532-3536.

St. Lawrence, W.F. and Cole, D.M., 1982. *Acoustic emissions from polycrystalline ice*. Cold Regions Science and Technology, 5, p. 183-199.

Appendix A – List of figures

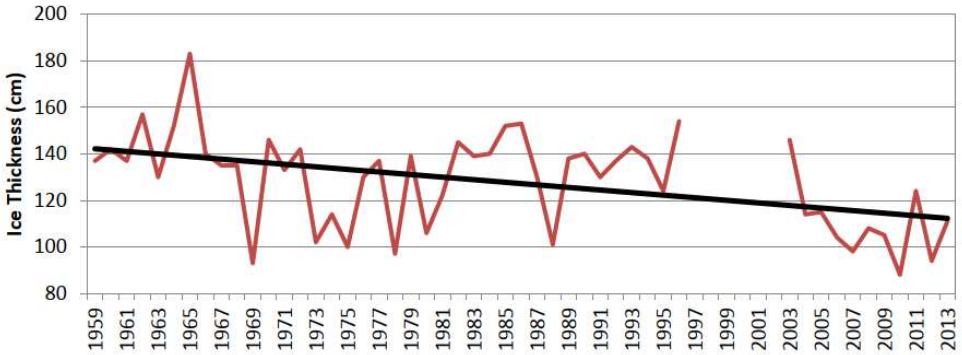

Figure 1: The variation in maximum annual ice thickness in the NWT near Yellowknife, based on data from Environment Canada, compiled by RSI (2014, Fig. 11).

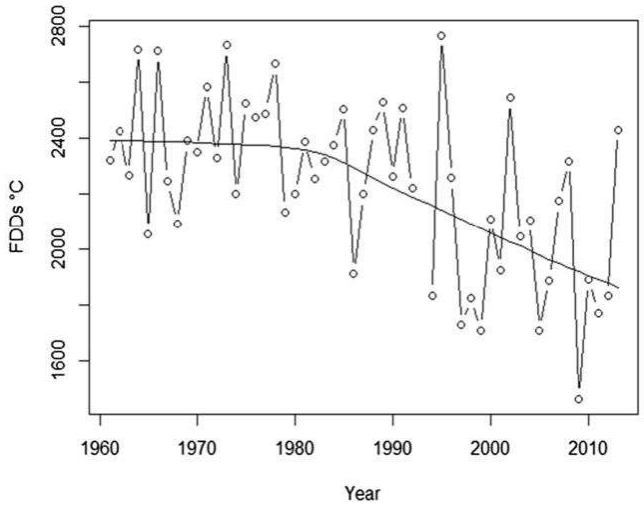

Figure 2: Reduction in the number of FDD in the James Bay region (Hori et al. , 2017).

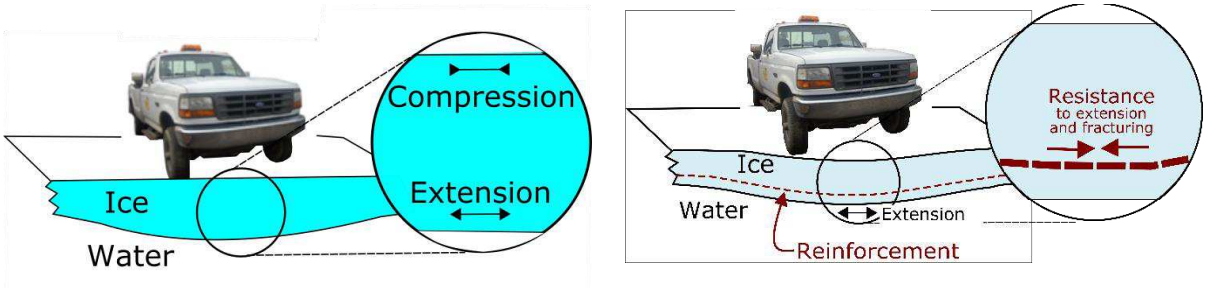

Figure 3: Left) Stress regime inside an ice cover loaded vertically. Right) Incorporation of a reinforcement inside an ice cover, to increase its resistance to the extensional component.

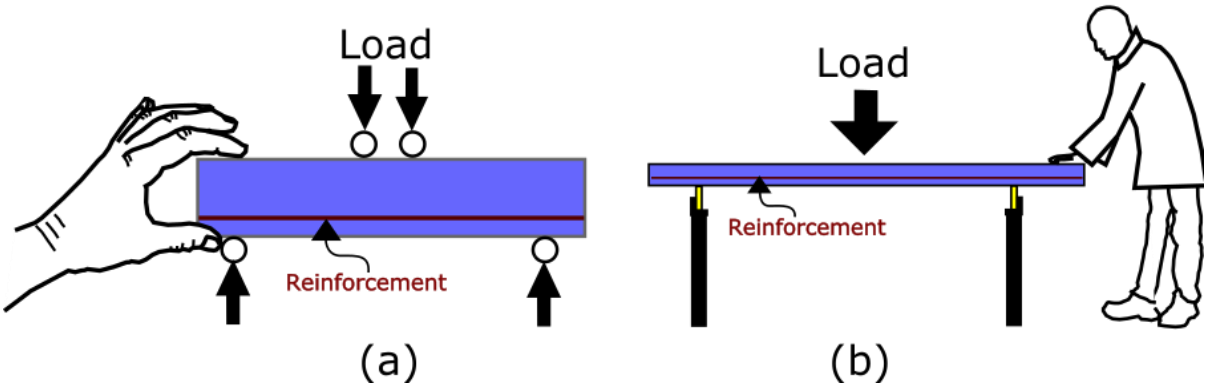

Figure 4: Two types of testing has been done: a) Phase 1, with rectangular beams (2D testing) – hand for scale; b) Phase 2, with plates of ice (3D testing) – person for scale.

Figure 5: Growth basin (1600 mm in length, 600 mm in width).

Figure 6: Set-up of reinforcement in the basin prior to bringing water into the basin. In this picture, the Stratagrid SG150 (left) and the threaded roads (right) are shown – these are discussed later.

Figure 7: Beam extraction from the growth basin.

Figure 8: A rough cut beam – this one does not have any reinforcement.

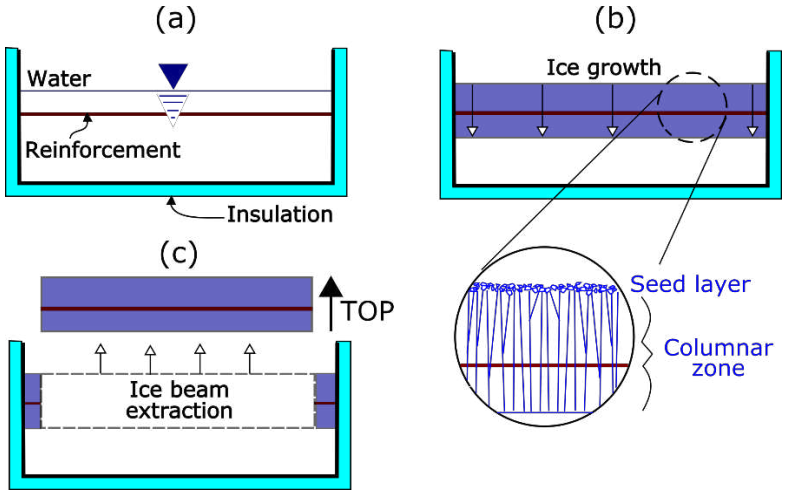

Figure 9: Ice growth (with reinforcement in this illustration): a) The reinforcement is set at the desired depth; b) Downward growth of columnar-grained ice; c) Beam extraction.

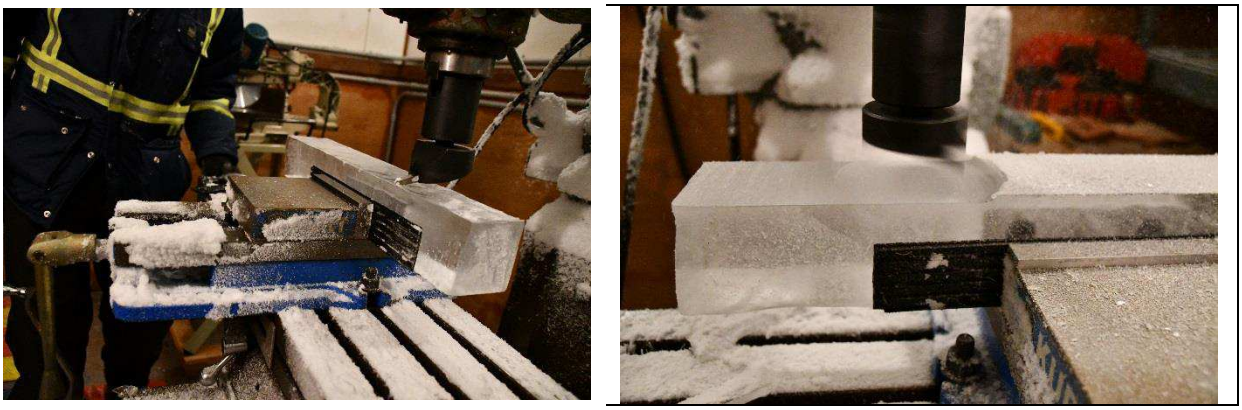

Figure 10 (left and right): Shaping the ice beams into the target testing dimensions with a lathe.

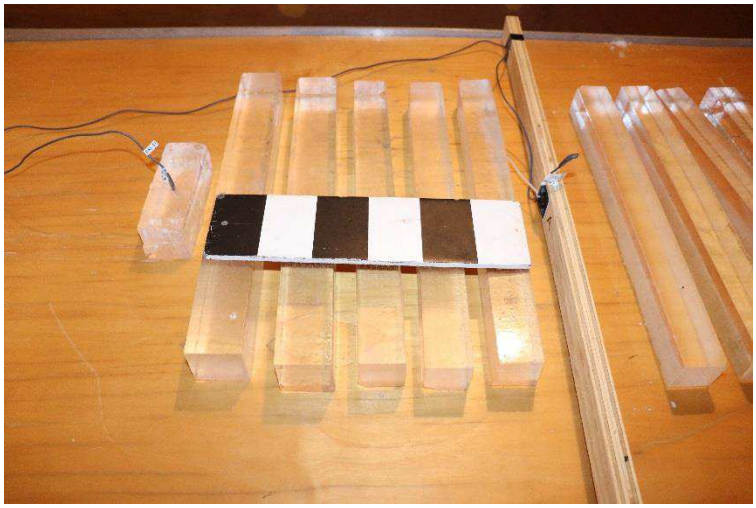

Figure 11: A set of beams machined to final dimensions, ready for testing. The partitions on the scale are 50 mm in width. Note on the left side, a dummy ice specimen with a temperature probe in it, to monitor ice temperature.

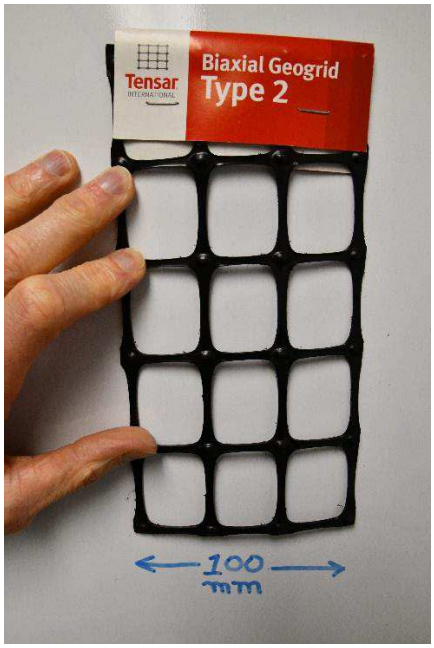

Figure 12: Sample of Tensar's biaxial Type 2 geogrid.

Figure 13: Sample of Stratagrid SG 150.

Figure 14: A 6 mm diameter threaded rod.

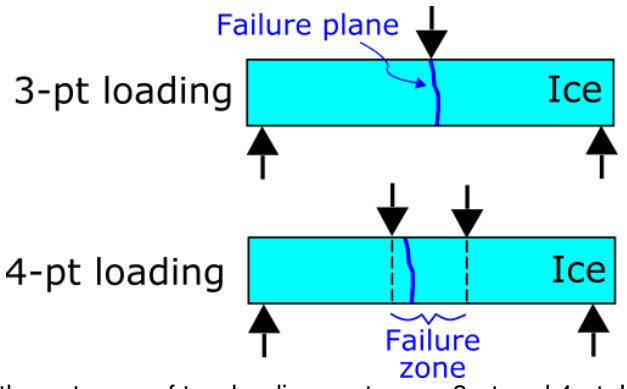

Figure 15: Difference in the outcome of two loading systems – 3-pt and 4-pt. In the first case, a failure plane has to occur below the top loading point; in the second case, it can occur anywhere inside the zone between the two upper loading points.

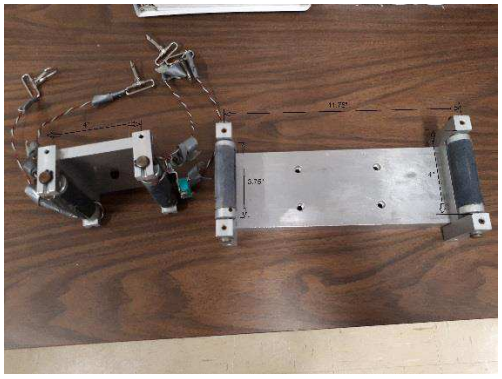

Figure 16: The load application frame (see Figure 18 for scale).

Figure 17: The un-instrumented Chatillon-type test frame (see Figure 18 for scale).

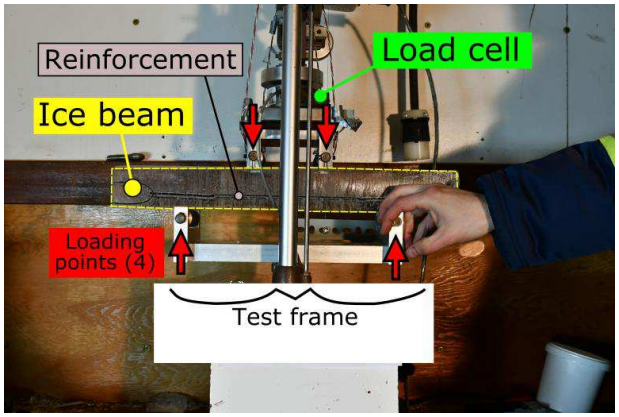

Figure 18: The Chatillon-type test frame about to apply the load on the ice beams (at the four points). Hand for scale. This example is for a reinforced ice beam.

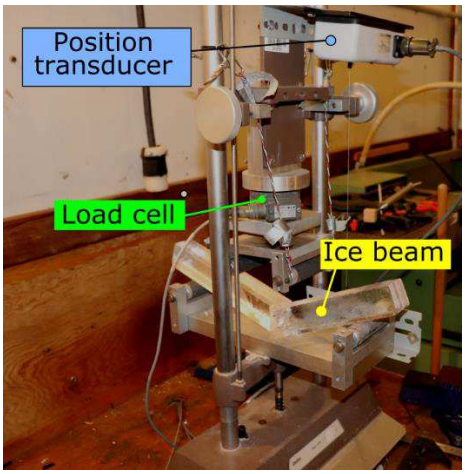

Figure 19: Same as previous figure but at a different angle, and after a test. See Figure 18 for scale.

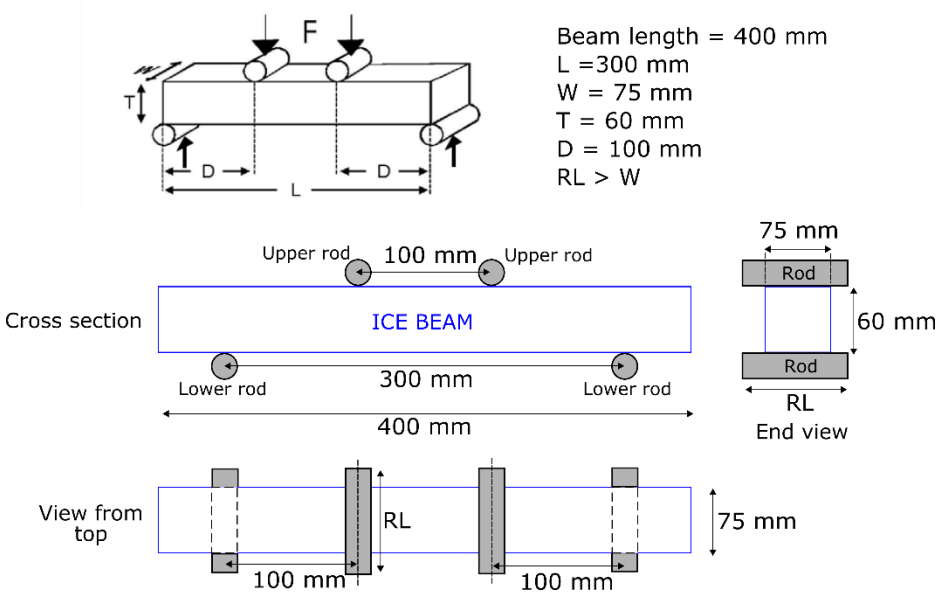

Figure 20: Beam testing configuration and target beam size. L: Beam length; W: Beam width; T: Beam thickness; D: Distance between upper and lower support; RL: Rod length.

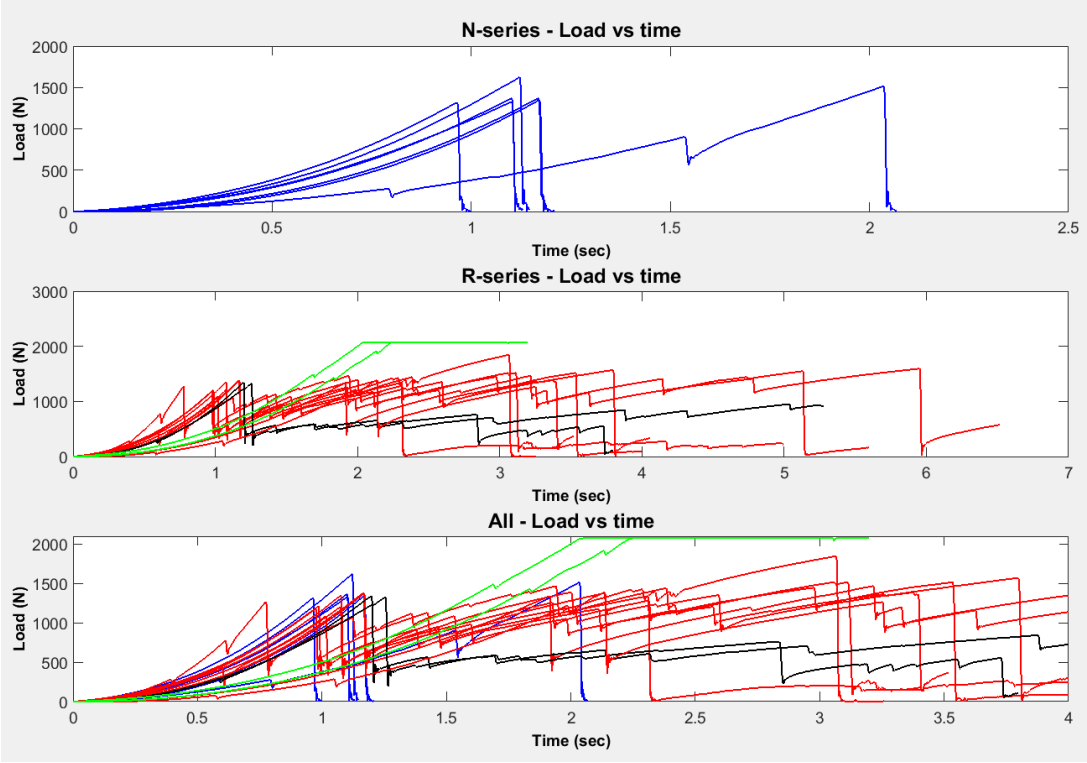

Figure 21: Load traces as a function of time for all tests – note the difference in time scale between the three plots. Blue traces are N-series; red traces are the R-series Tensar Type 2 reinforcement; black traces are with the R-series Stratagrid SG 150 material; green traces are with the R-series threaded rods.

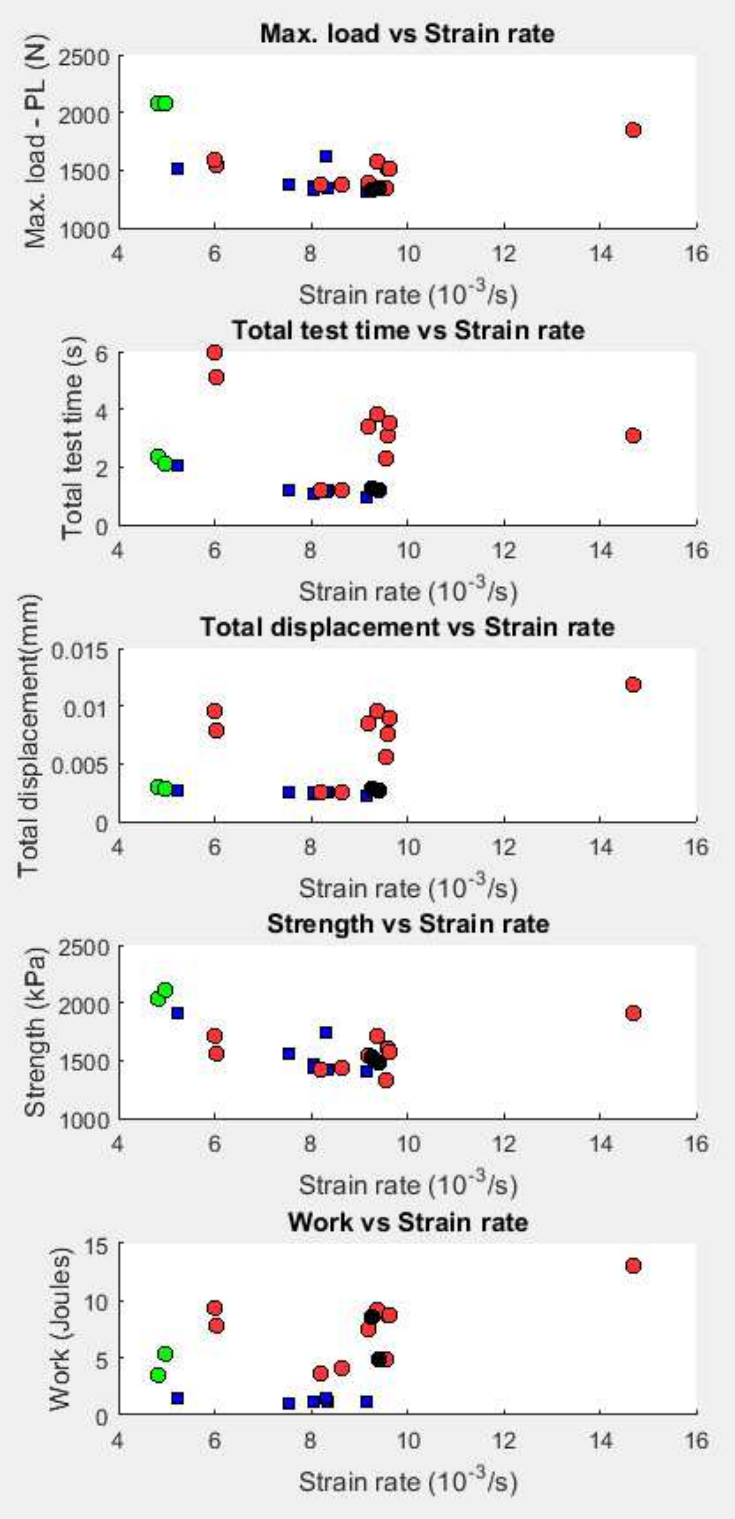

Figure 22: The various parameters plotted against displacement rate. Blue squares are N-series; red circles are Tensar-reinforced; black circles are Stratagrid-reinforced; green circles are the threaded rods-reinforced.

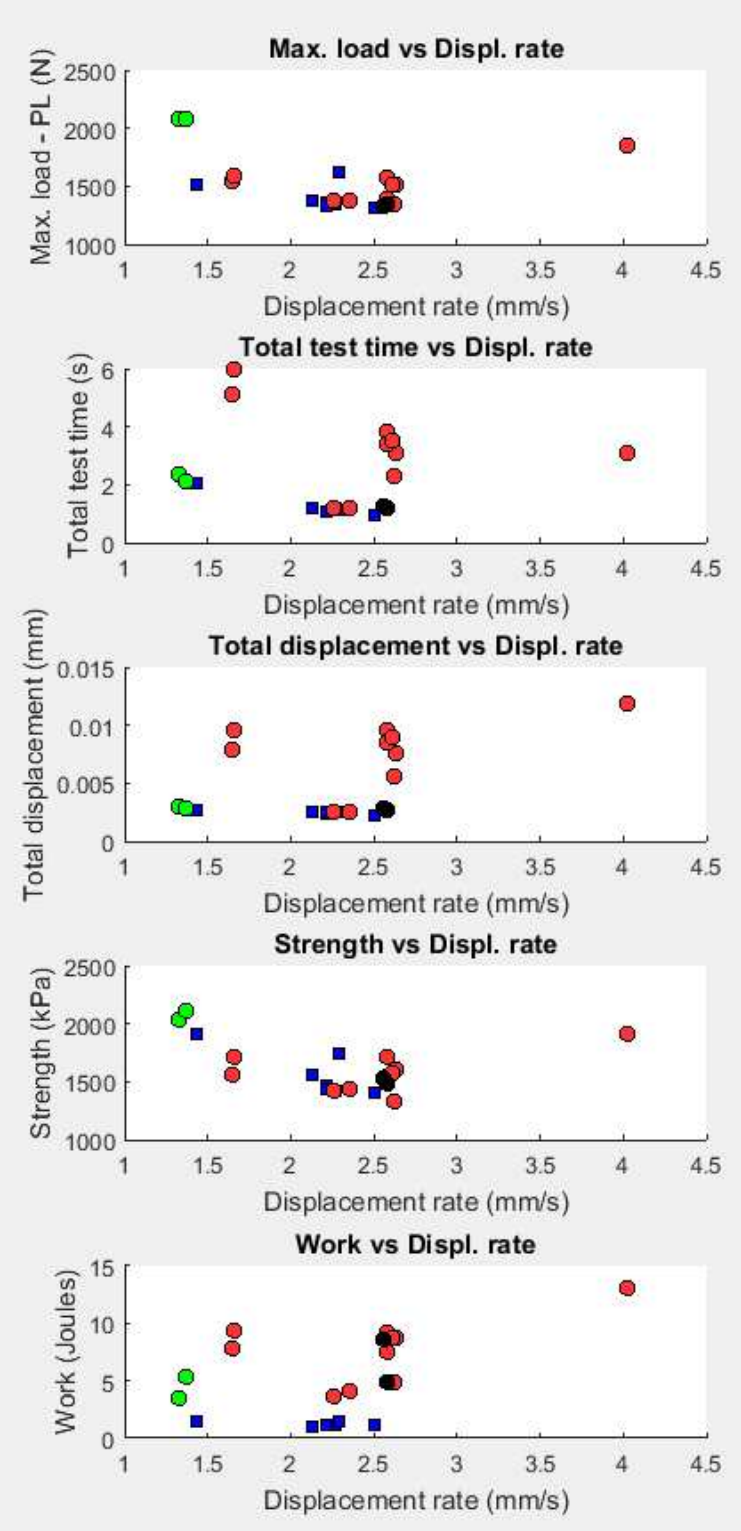

Figure 23: The various parameters plotted against strain rate. Blue squares are N-series; red circles are Tensar-reinforced; black circles are Stratagrid-reinforced; green circles are the threaded rods-reinforced.

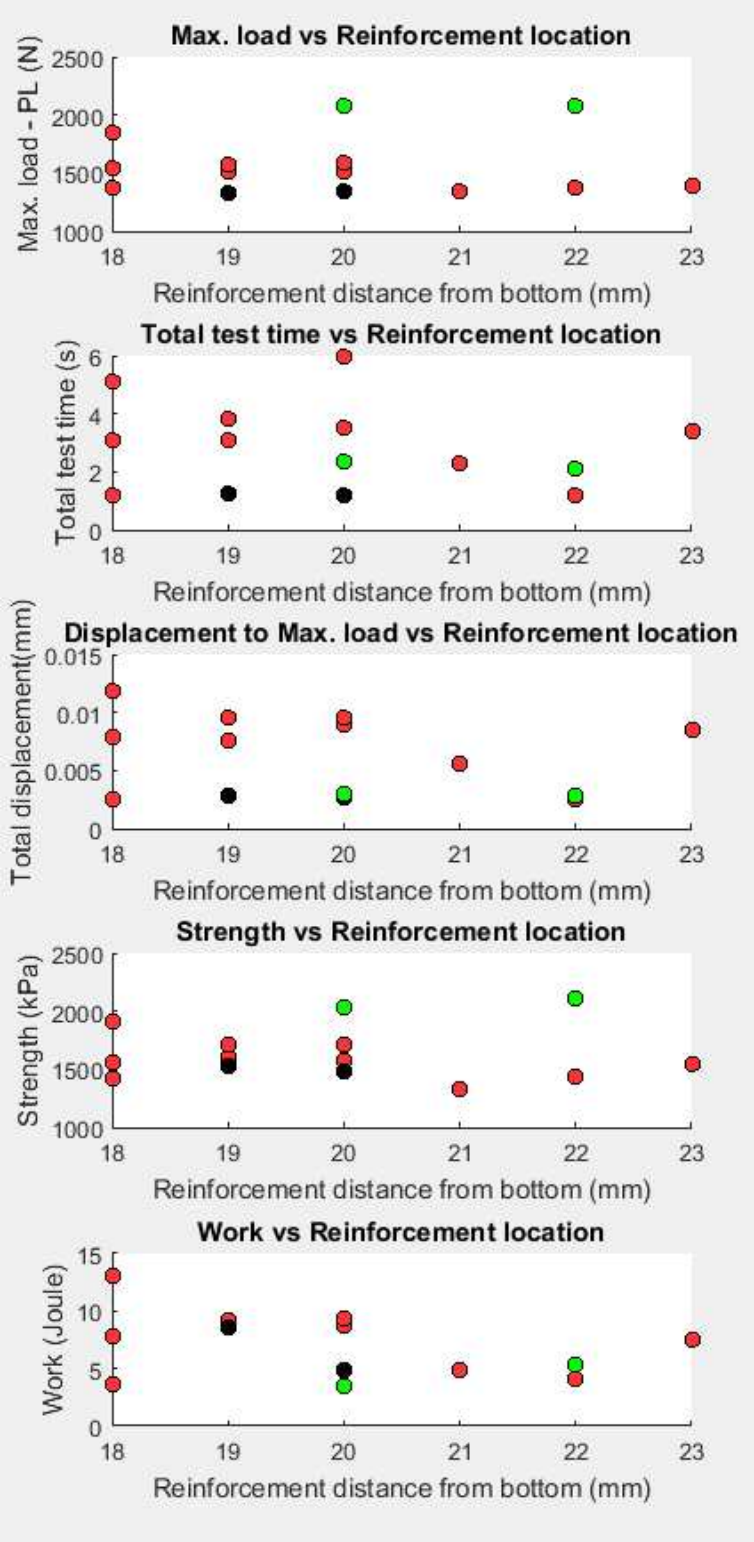

Figure 24: The various parameters (for R-series only) plotted the distance between the reinforcement and the bottom surface of the beam. Red circles are Tensar-reinforced; black circles are Stratagrid-reinforced; green circles are the threaded rods-reinforced.

Figure 25: A test beam is cut with a band saw.

Figure 26: The band saw surface is smoothened on a 100 grit sanding mesh.

Figure 27: The ice returns to the band saw, and a slice of ice is cut with the smooth surface against the platen.

Figure 28: The outcome is an ice slice whose smooth surface is later spot welded onto a clean glass plate with drops of water.

Figure 29: The glass plate and the ice slice are installed onto the microtome.

Figure 30: A closer look of the ice spot-welded onto the glass plate. The microtome knife at the right shaves thin layers of ice up to a point where that ice surface becomes perfectly smooth.

Figure 31: The ice/glass assembly is then flipped upside down onto another clean glass plate (i.e. with the microtomed surface against it), and while applying a slight downward pressure on it, a bead of water is run along the full perimeter (using a plastic eye dropper).

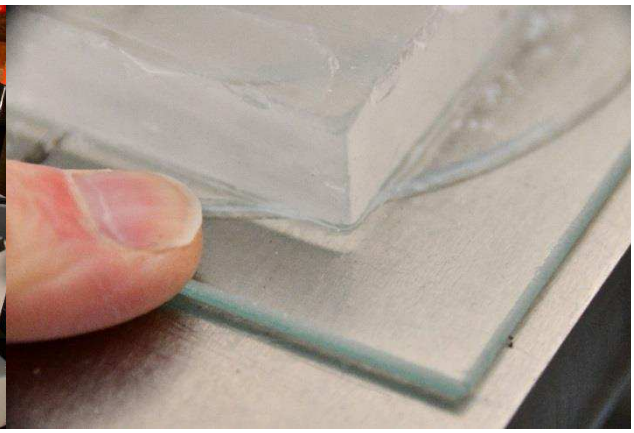

Figure 32: A close-up of the bead around the ice. This is a critical step – if the procedure is well done, no water will make its way between the ice and the glass.

Figure 33: The thickness of the ice slab is reduced by melting it against a plate of aluminum at room temperature (i.e. brought in from outside the cold room). The ice/glass assembly is then returned to the microtome, which is used to further thin the ice (by repeated shaving) to a target thickness of one millimeter.

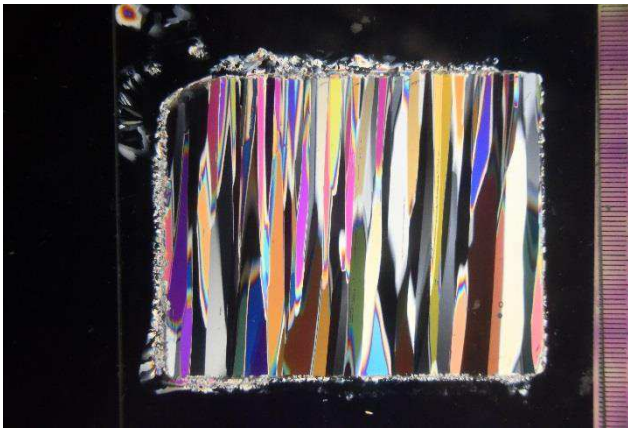

Figure 34: Cross (vertical) section of columnar-grained ice seen through crossed-polarized light. Up is the top of the ice cover – note how the grains become progressively wider toward the bottom (a growth competing process). The scale along the right edge of the photograph is graded in millimeters.

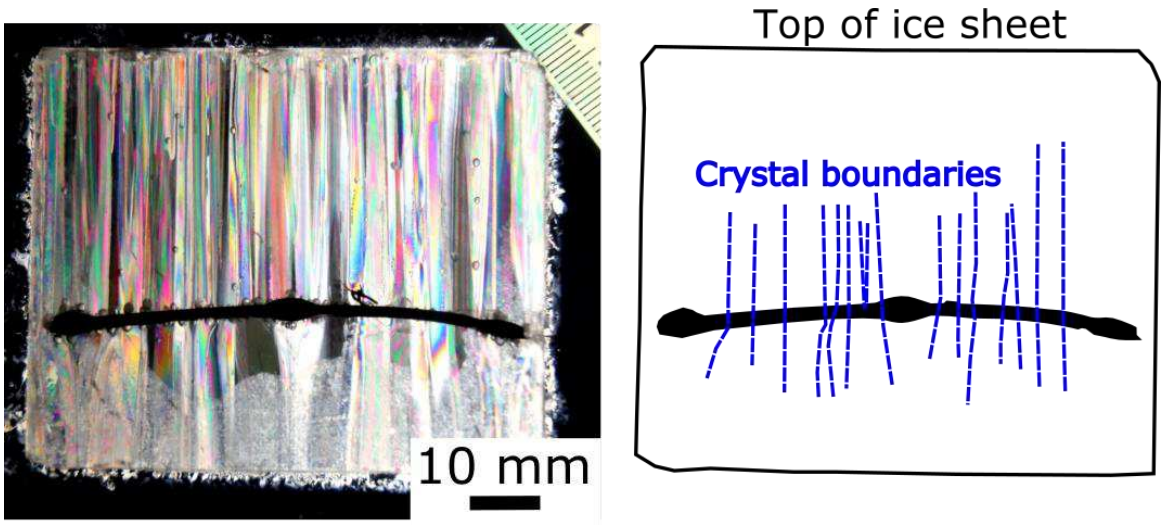

Figure 35 - Left) Thin section in cross-polarized light across the thickness of an ice cover, with the enclosed Tensar geogrid. Right) Outline of crystal boundaries and membrane. Note how the crystal are able to grow through the membrane, i.e. the membrane does not promote a discontinuity.

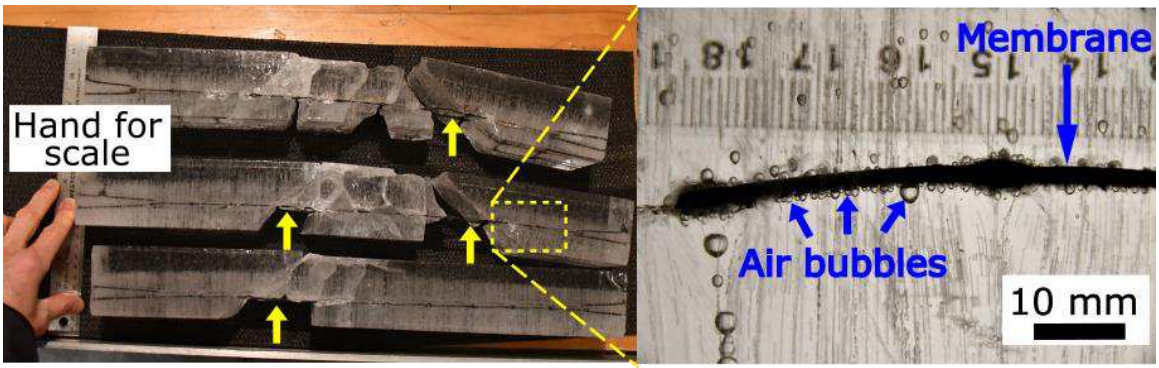

Figure 36 - Above left) Three reinforced beams after breakage pointing to a cleavage surfaces (arrows). Above right) Close-up (in thin section under plain light) of the interface between the geogrid and the ice. Note the presence of air bubbles – these could be responsible for the cleavage.

Figure 37: Thin section in cross-polarized light, cut across the membrane. As before, it shows that the crystal are able to grow ‘through’ the membrane. Scale in millimeter.

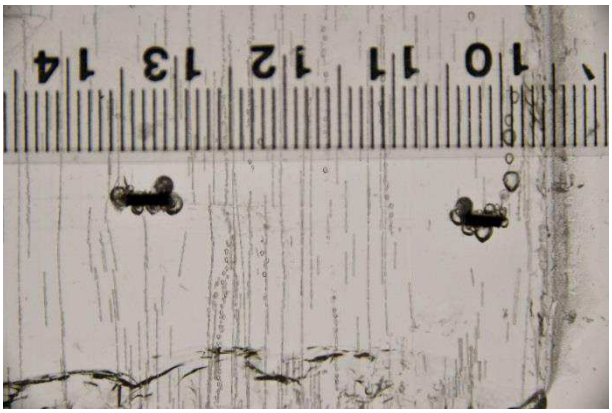

Figure 38: The same as in the previous figure, but under plain light, which shows the air entrapment that have nucleated around the membrane. Scale in millimeter.

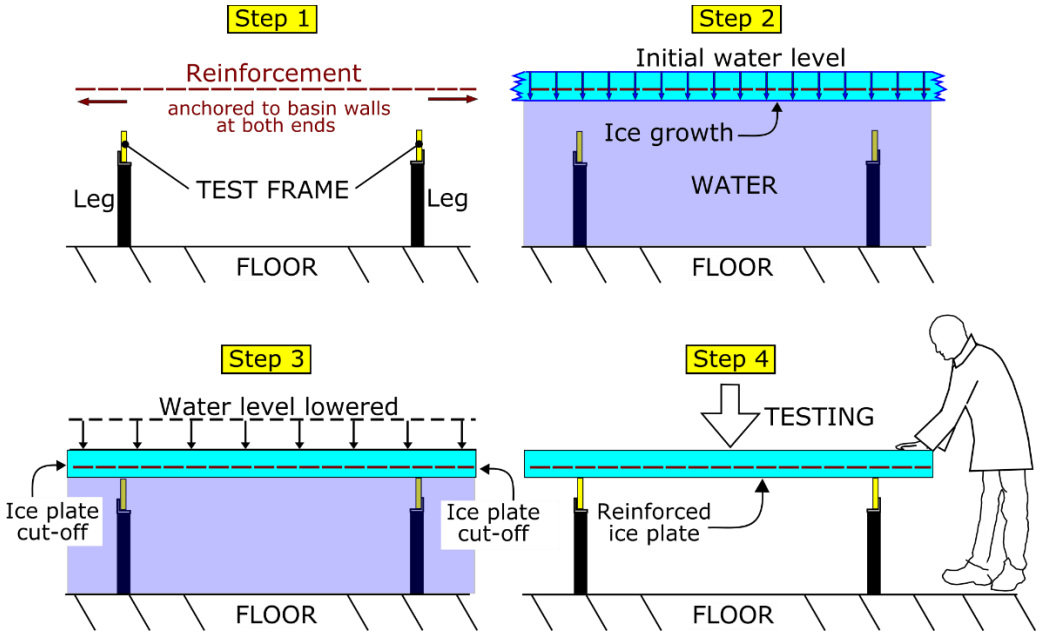

Figure 39: Four-step procedure used for plate testing. Step 1: Installation of test frames and reinforcement in the ice tank. Step 2: Water in the ice tank and freeze up of a sheet around the reinforcement. Step 3: Cut-off of the ice around the frame into a plate, and lowering of that ice onto the test frame. Step 4: Removal of remaining water and testing.

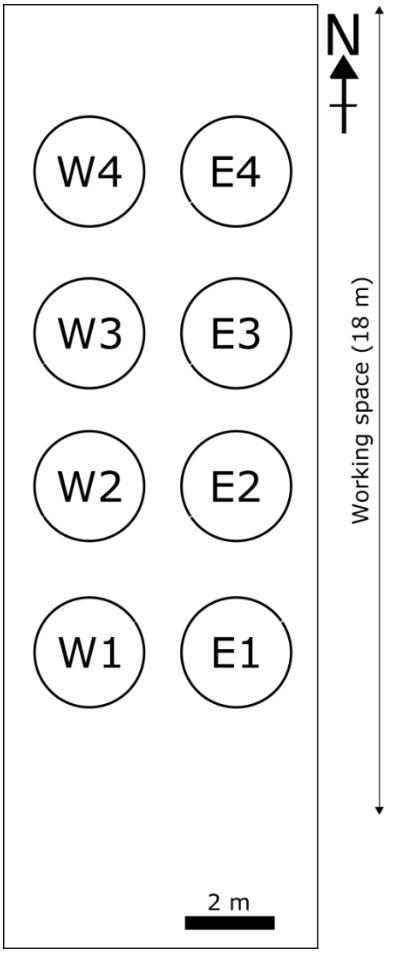

	N-S	E-W
	Diameter (millimeters)	
E1	2503	2537
E2	2524	2477
E3	2523	2522
E4	2520	2532
W1	2532	2480
W2	2522	2492
W3	2505	2539
W4	2519	2525
Average	**2519**	**2513**

Figure 40: Left) Layout of the eight loading frames inside the ice tank, and the labels used for each test. The tank is 21 meter is length by 7 meters in width (to scale). Right) The frames' external diameter along the N-S and E-W directions. All outside perimeters were 7.92 meters.

Figure 41: The eight circular test frames (yellow) are deployed inside the ice tank. The person at far back is for scale.

Figure 42: Examples of reinforcement layouts over the test frames. Person for scale again.

Figure 43: The tank filled with water.

Figure 44: 'Seeding' event at 15°C – the mist in the air is made from tiny crystals that settle on the water surface and initiate ice growth.

Figure 45: After the seeding event, the water surface is covered with a thin ice layer, which then grows downward (see Figure 9). On the left, next to the two people, is one of the two rails the carriage travels on.

Figure 46: Once the ice above the test frames had achieved target thickness (thereby incorporating the reinforcement), it was cut around each test frame. This was done from the carriage that spans the width of the basin.

Figure 47: Individual plates after having been cut and the water level having been lowered, bringing them down and allowing them to rest directly on the test frames. Person for scale upper left corner.

Figure 48: The carriage has been move to the location of a test. Below it is the instrumentation used to monitor the ice loading event and the ice response. Person with orange jacket for scale, upper right.

Figure 49: Piston viewed from above. The circular platen (stainless steel) at its end can be seen below the (blue) load cell.

Figure 50: General view of the set-up on the carriage – the worker below the other people is standing on the floor of the ice tank, inside a test frame.

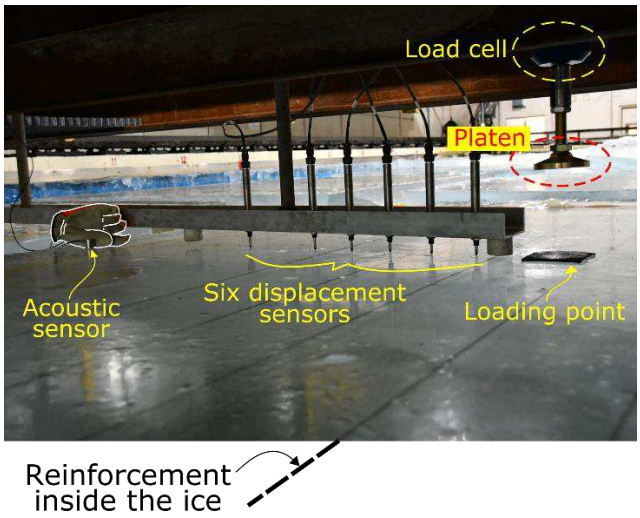

Figure 51: Below the carriage, instrumentation set-up before a test on ice reinforced with steel cables (glove for scale on the left).

Figure 52: After the test – the indentation event caused the ice to fail mostly via a series of radial cracks.

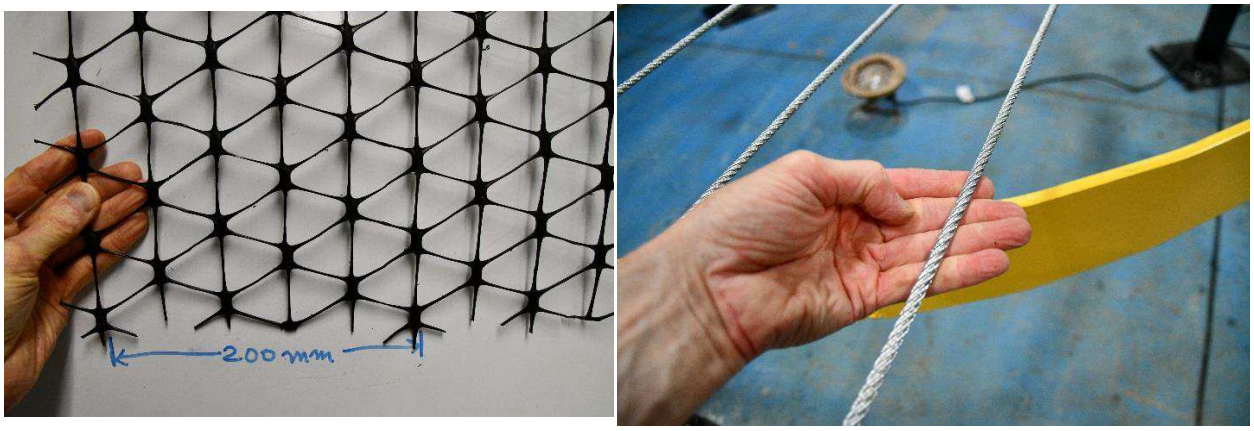

Figure 53: The two reinforcement material used for plate testing: Left) Tensar's triaxial TX7 geogrid; right) Steel cable – this one is 6.4 mm in diameter.

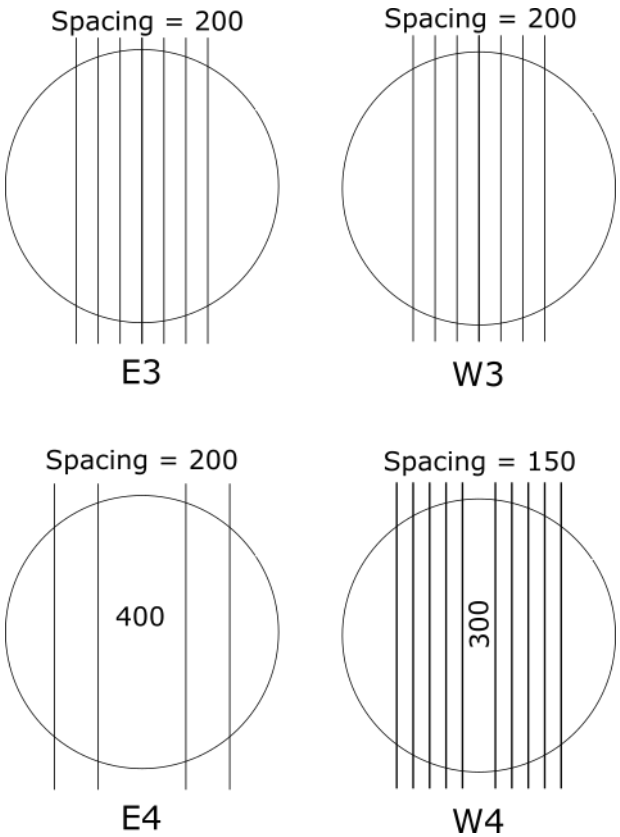

Figure 54: Layout of steel cables. Spacing is in millimeters, all sets are centered with the frame. The circle is the test frame, with a nominal diameter of 2500 mm.

Figure 55: Load frame E2 with the geogrid laid out above it.

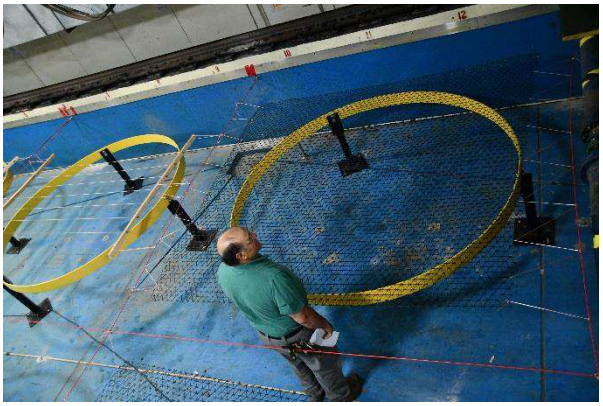

Figure 56: Same as previous.

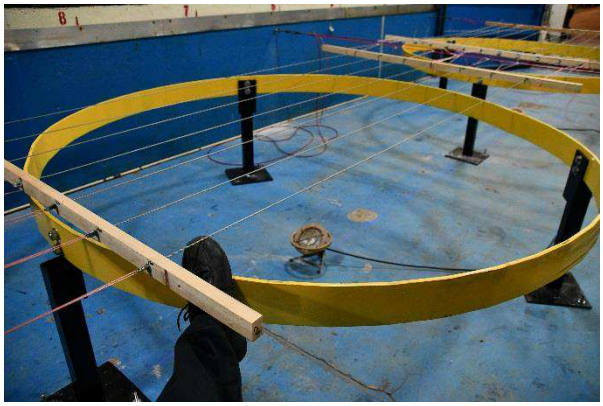

Figure 57: Reinforcement layout – W4 is used here as an example. Note the steel strands are several centimeters above the yellow frame.

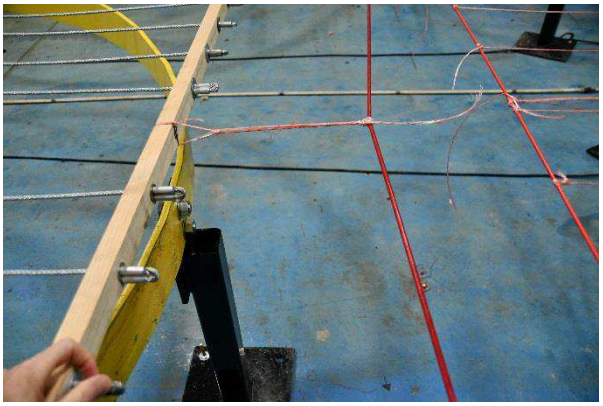

Figure 58: Close-up of reinforcement layout – with W4 again. The red lines were used to apply a tension. The wood onto which are attached the reinforcement cables is tied to that line with plastic cables.

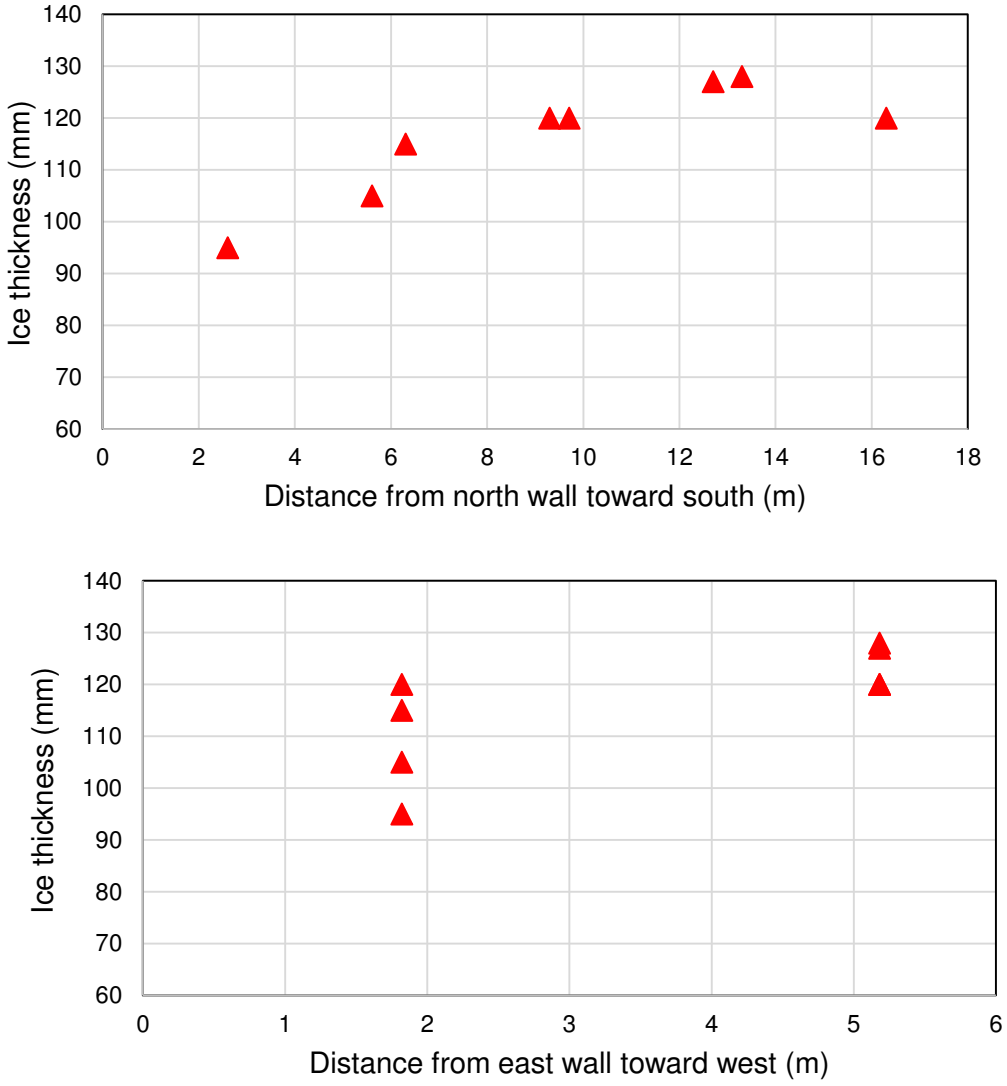

Figure 59: Ice thickness variation across the ice tank. The upper plot shows the variation along the length of the ice tank; the lower plot shows a variation across its width.

Figure 60: Example (W4) showing cables out of the ice plate at bottom before testing.

Figure 61: Polypropylene geogrid inside the ice before test E1 – note the presence of air bubbles along the ice-material interface.

Figure 62: Cables in the ice, also where air entrapment tends to accumulate.

Figure 63: A thermistor profiler was used to keep track of temperature inside and outside the ice.

Figure 64: Circular indentor used for load application. It is connected to a threaded rod via a universal joint.

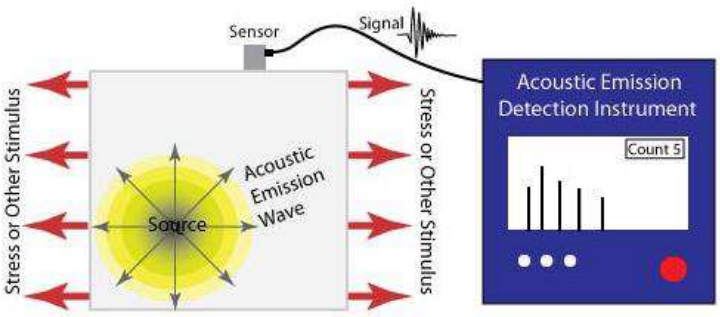

Figure 65: Energy is emitted from a crack (the source) in all directions, in the form of an AE wave, which is detected by a sensor at the surface. [Source: NDT Resource Centre]

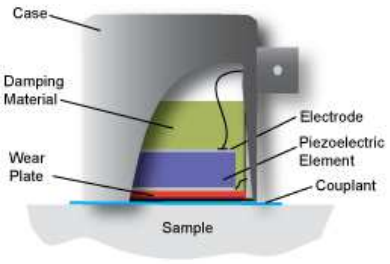

Figure 66: Typical configuration of an AE sensor [Source: NDT Resource Centre].

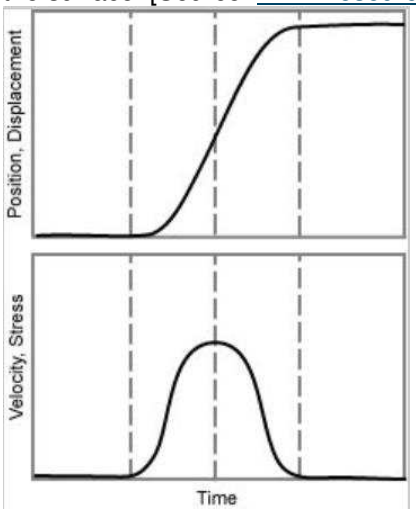

Figure 67: Top) A wave associated with the formation of a crack, the later expressed as a position/displacement as a function of time. Bottom) The wave is also associated with a transient, or recoverable, motion or stress in the material, which reaches a maximum before reversing to zero [Source: NDT Resource Centre]

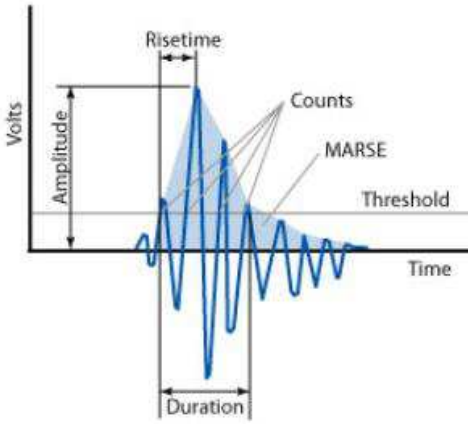

Figure 68: AE event on a volt vs time plot. [Source: NDT Resource Centre] See text for explanations.

Figure 69: Our AE sensor frozen onto the ice surface of a reinforced ice plate ready to be tested (finger for scale).

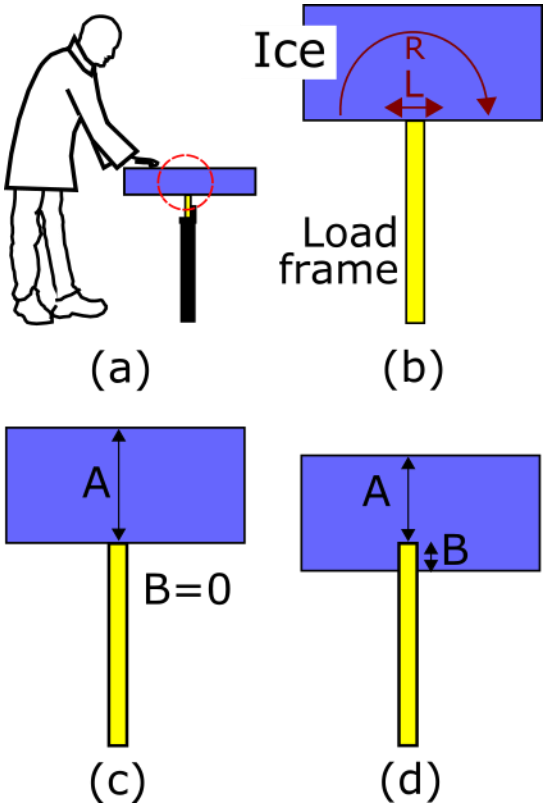

Figure 70: In this study, the nature of the interaction between the ice plate and the load frame (a) led to a different levels of restriction along that interface. As shown in (b), these are divided into: rotational (R) and lateral (L). See text for discussion. In (c), the ice lies on top of the frame; in (d), the frame melted its way into the ice. A is the thickness of the ice above the frame, and B is the penetration depth.

Appendix B – Plate deflection in response to loading

This appendix contains a graphical representation of the main instrumentation output: the piston/platen displacement, the load cell and the displacement from each of the six displacement transducers. The test number is indicated above all plots.

In the upper plot, all of the instrumentation output is shown. Displacements and load are plotted against time. Displacements are indicated on the left-hand y-axis for all LVITs and the platen. Load is indicated on the right-hand y-axis.

In the lower plot, the output of the six LVITs are shown as a function of distance away from the loading point. A ‘snap shot’ of plate deflection at three time intervals are indicated. The purpose of this plot is to help validate numerical modeling, to be done later, for the short-term response.

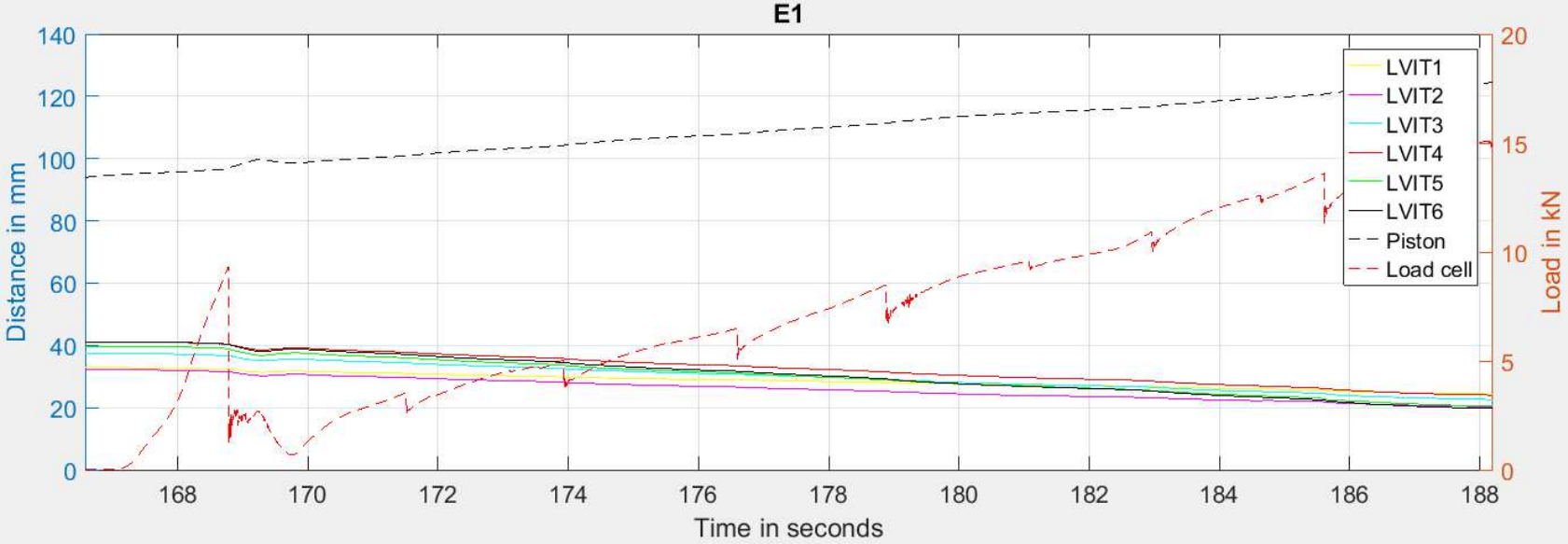
E1
Distance in mm
Load in kN
Time in seconds
LVIT1
LVIT2
LVIT3
LVIT4
LVIT5
LVIT6
Piston
Load cell
0
20
40
60
80
100
120
140
0
5
10
15
20
168
170
172
174
176
178
180
182
184
186
188

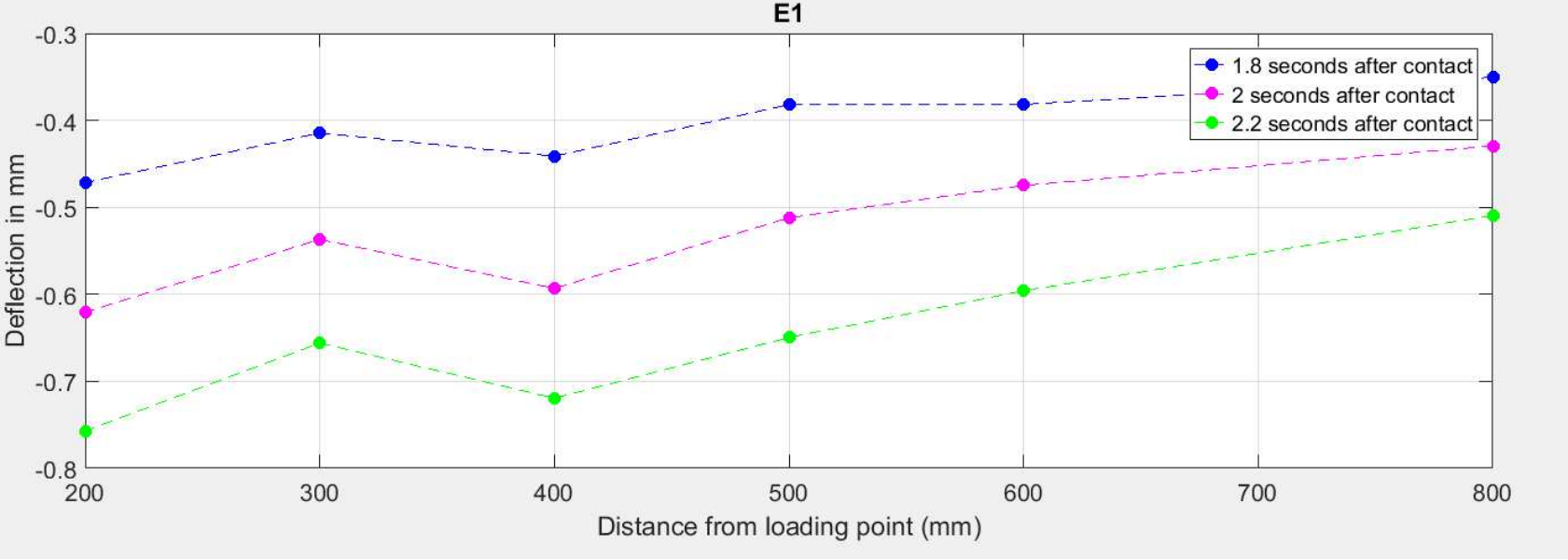
E1
Deflection in mm
Distance from loading point (mm)
1.8 seconds after contact
2 seconds after contact
2.2 seconds after contact
-0.3
-0.4
-0.5
-0.6
-0.7
-0.8
200
300
400
500
600
700
800

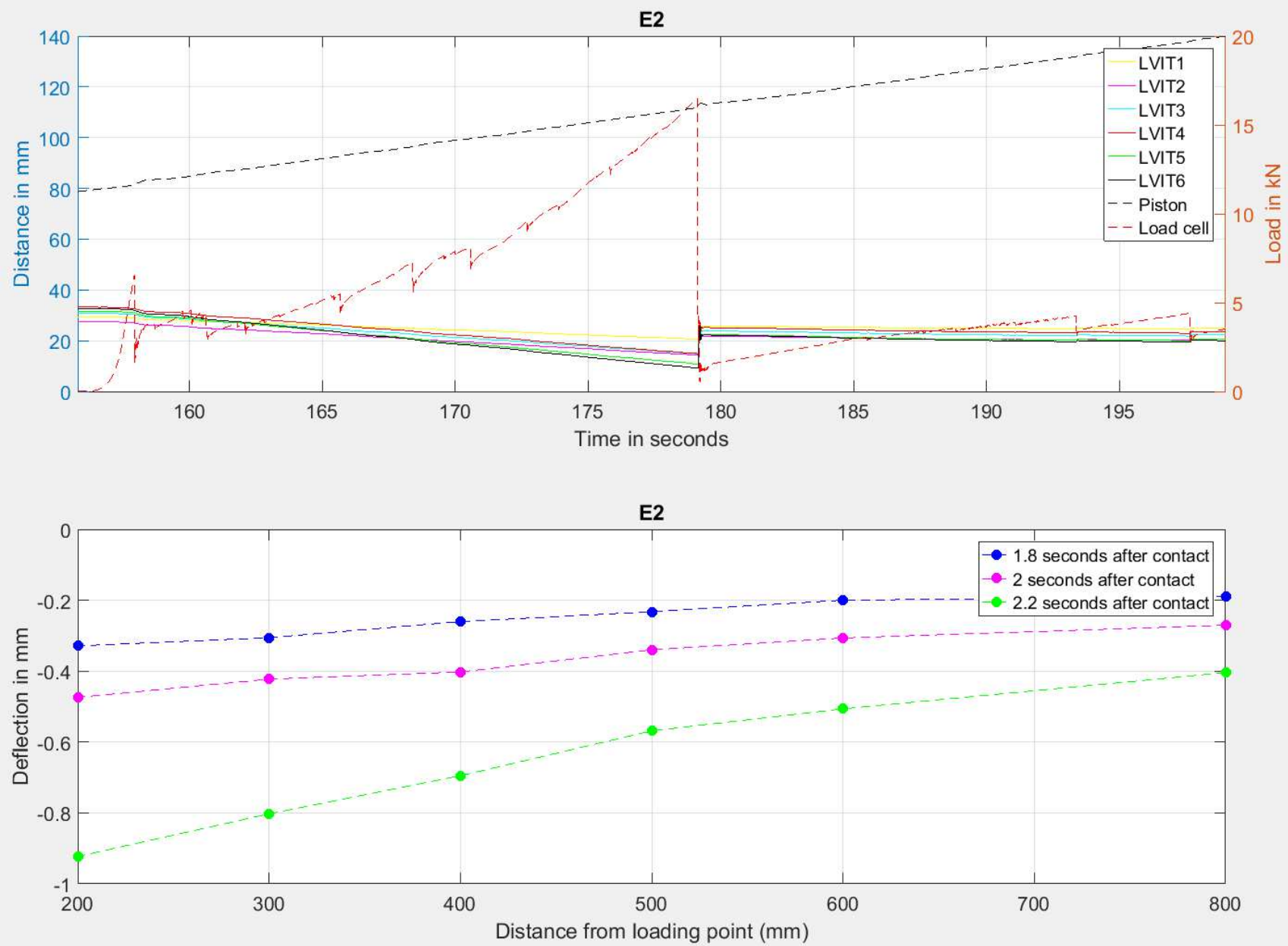
E2
Distance in mm
Load in kN
Time in seconds
LVIT1
LVIT2
LVIT3
LVIT4
LVIT5
LVIT6
Piston
Load cell
E2
Deflection in mm
Distance from loading point (mm)
1.8 seconds after contact
2 seconds after contact
2.2 seconds after contact

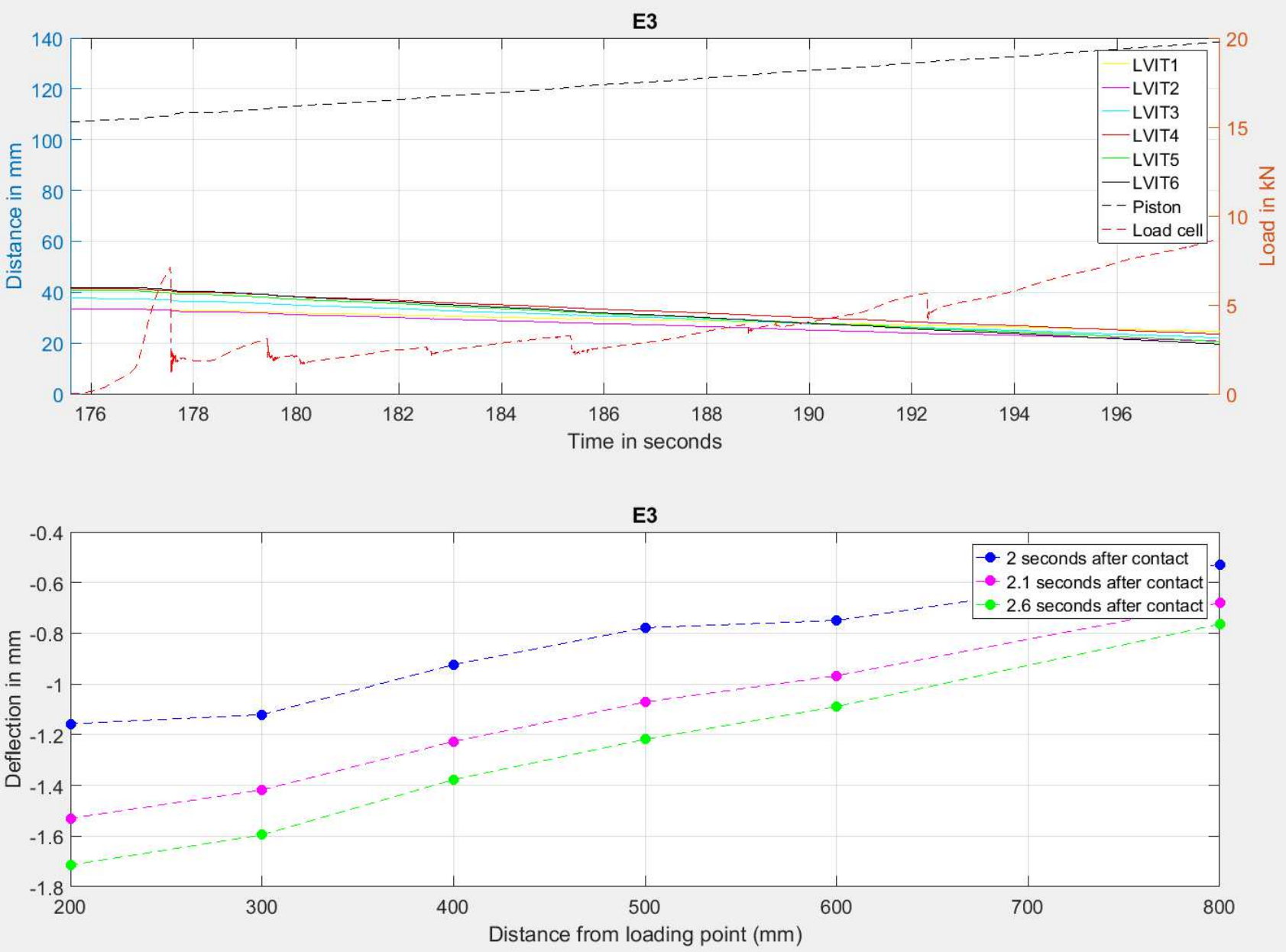
E3
Distance in mm
Load in kN
Time in seconds
LVIT1
LVIT2
LVIT3
LVIT4
LVIT5
LVIT6
Piston
Load cell
E3
Deflection in mm
Distance from loading point (mm)
2 seconds after contact
2.1 seconds after contact
2.6 seconds after contact

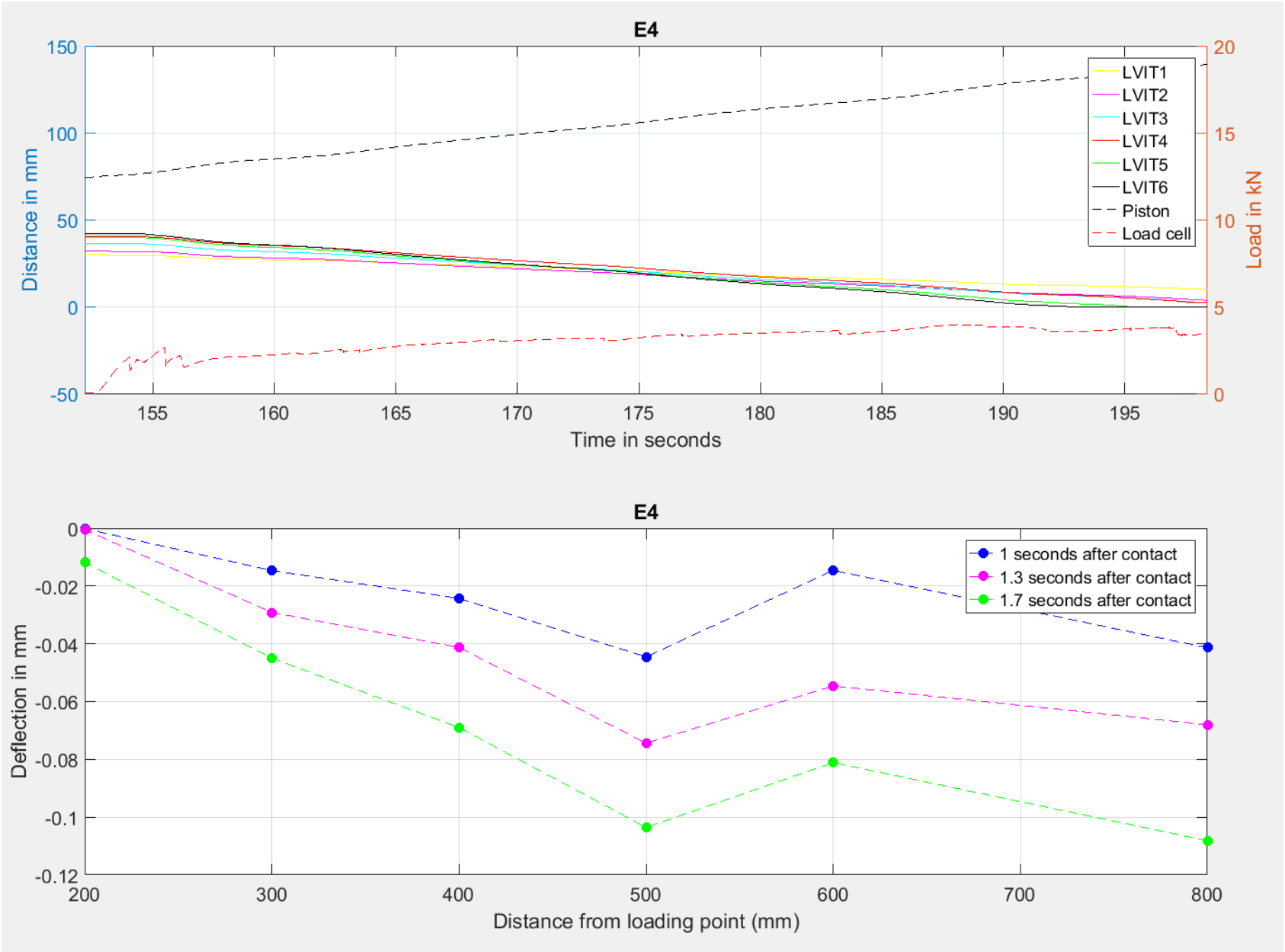
E4
Distance in mm
Load in kN
Time in seconds
LVIT1
LVIT2
LVIT3
LVIT4
LVIT5
LVIT6
Piston
Load cell
150
100
50
0
-50
20
15
10
5
0
155
160
165
170
175
180
185
190
195
E4
Deflection in mm
Distance from loading point (mm)
1 seconds after contact
1.3 seconds after contact
1.7 seconds after contact
0
-0.02
-0.04
-0.06
-0.08
-0.1
-0.12
200
300
400
500
600
700
800

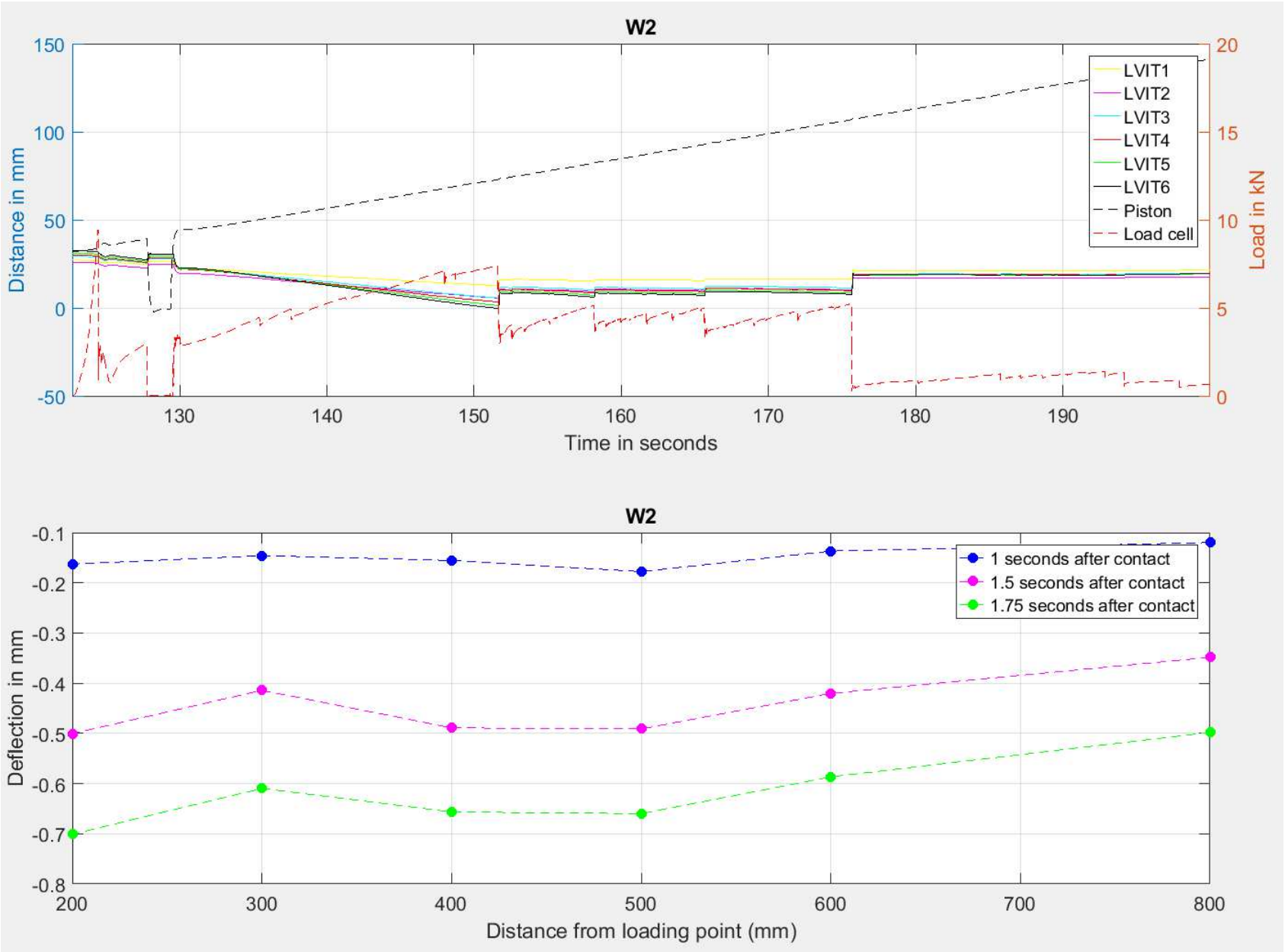
W2
Distance in mm
Load in kN
Time in seconds
LVIT1
LVIT2
LVIT3
LVIT4
LVIT5
LVIT6
Piston
Load cell
W2
Deflection in mm
Distance from loading point (mm)
1 seconds after contact
1.5 seconds after contact
1.75 seconds after contact

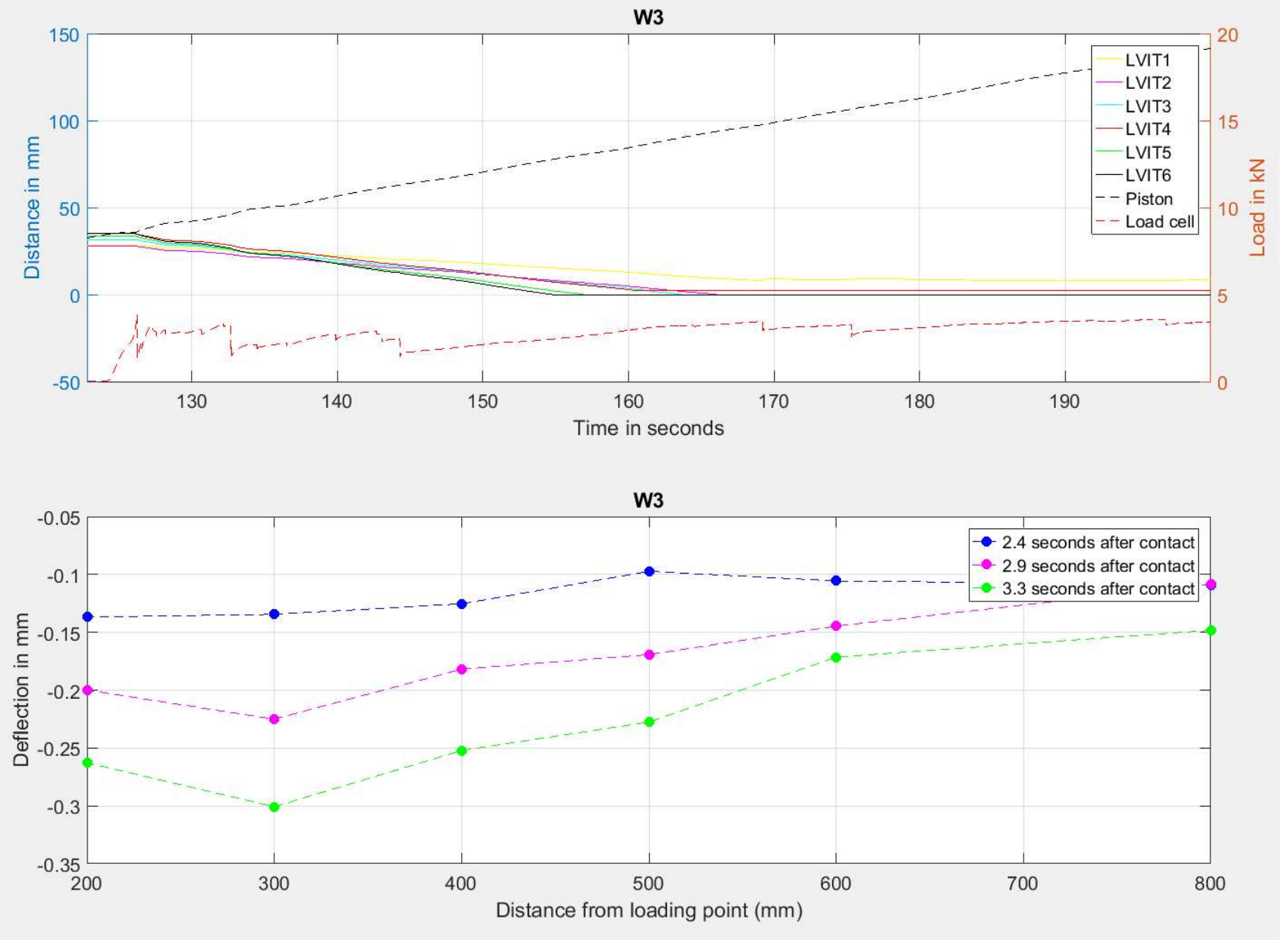
W3
Distance in mm
Load in kN
Time in seconds
LVIT1
LVIT2
LVIT3
LVIT4
LVIT5
LVIT6
Piston
Load cell
W3
Deflection in mm
Distance from loading point (mm)
2.4 seconds after contact
2.9 seconds after contact
3.3 seconds after contact

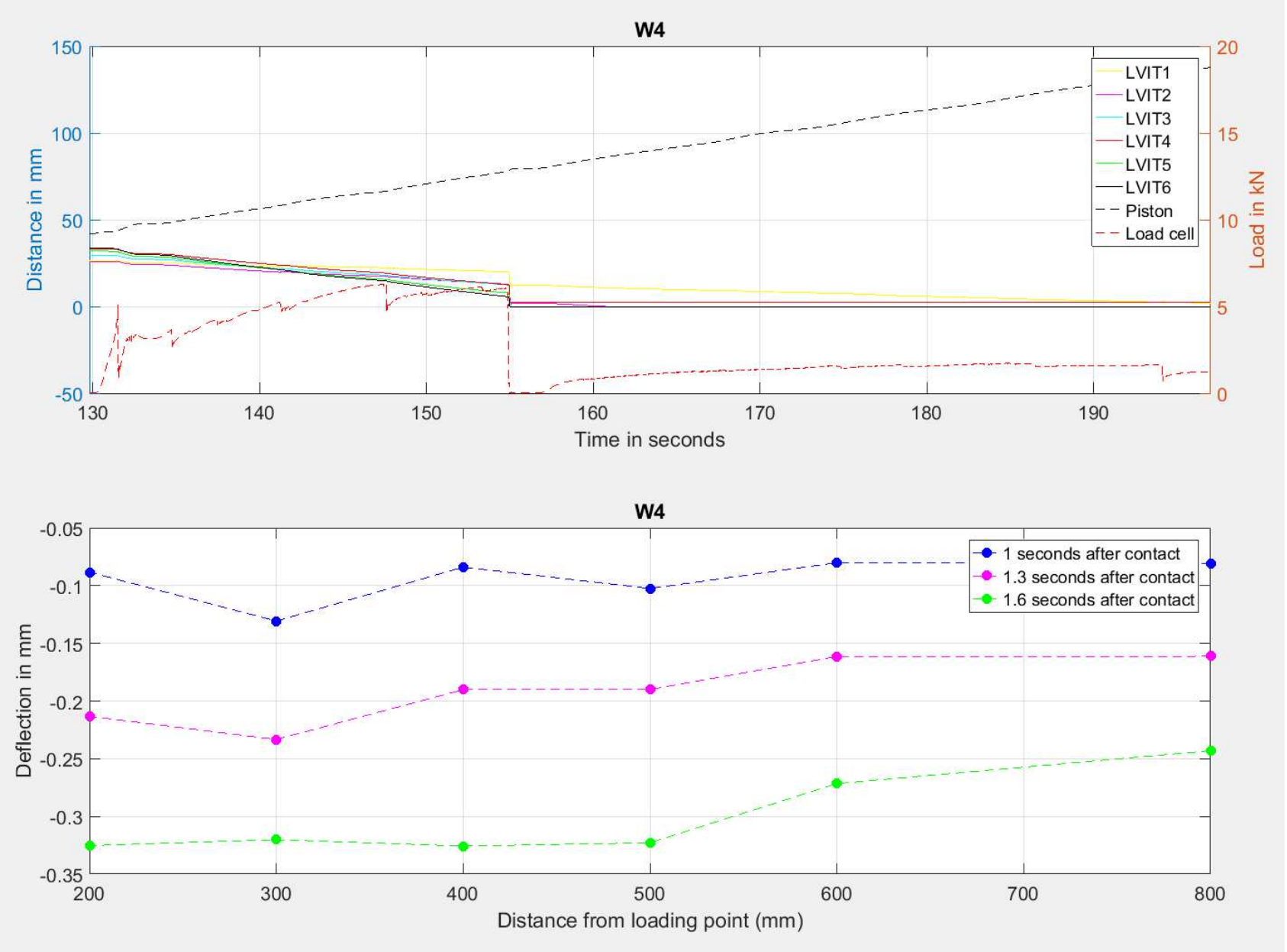
W4
Distance in mm
Load in kN
Time in seconds
LVIT1
LVIT2
LVIT3
LVIT4
LVIT5
LVIT6
Piston
Load cell
W4
Deflection in mm
Distance from loading point (mm)
1 seconds after contact
1.3 seconds after contact
1.6 seconds after contact

Appendix C – Acoustic sensor response in response to loading

This appendix contains a graphical representation of the load cell output, piston/platen displacement and acoustic sensor output. The test number is indicated above the plots.

In the upper plot, platen displacement and load are plotted against time – the former is indicated on the left-hand y-axis; the latter is indicated on the right-hand y-axis. In the lower plot, the acoustic sensor response is plotted along the same time scale as that indicated in the upper plot.

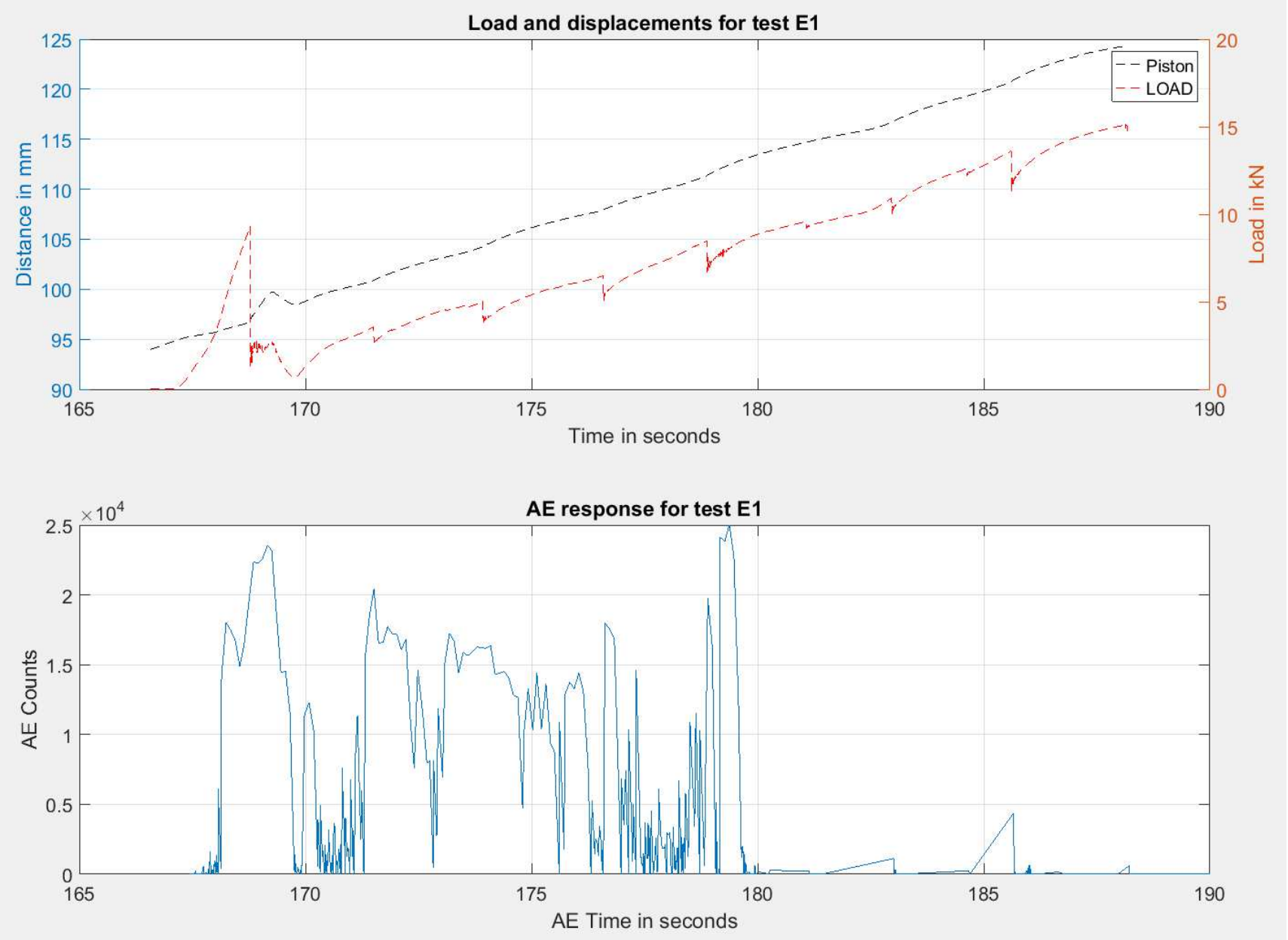
Load and displacements for test E1
Distance in mm
Load in kN
Time in seconds
Piston
LOAD
125
120
115
110
105
100
95
90
20
15
10
5
0
165
170
175
180
185
190
AE response for test E1
×10^4
AE Counts
AE Time in seconds
2.5
2
1.5
1
0.5
0

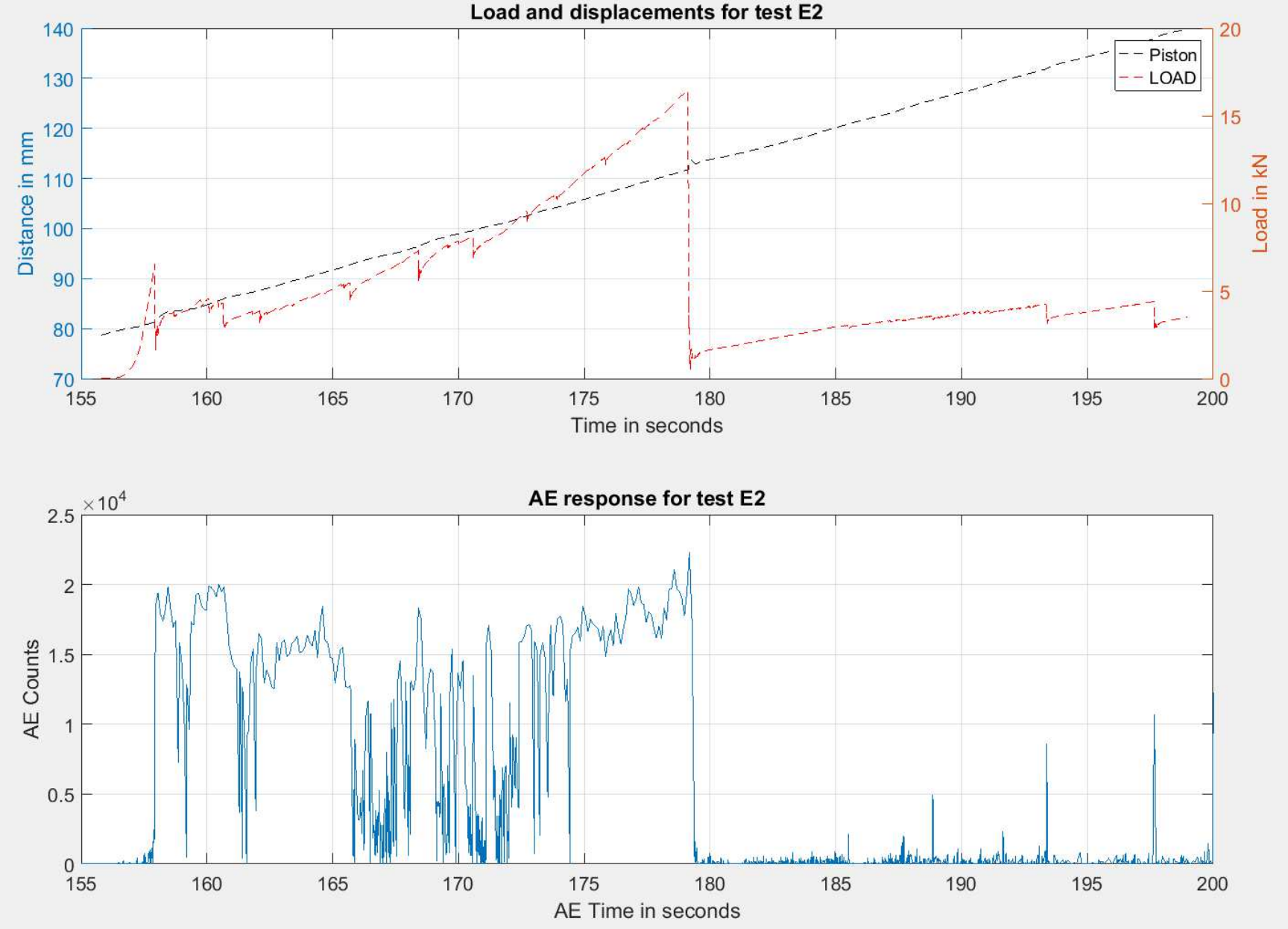
Load and displacements for test E2
Distance in mm
Load in kN
Time in seconds
Piston
LOAD
AE response for test E2
×10^4
AE Counts
AE Time in seconds

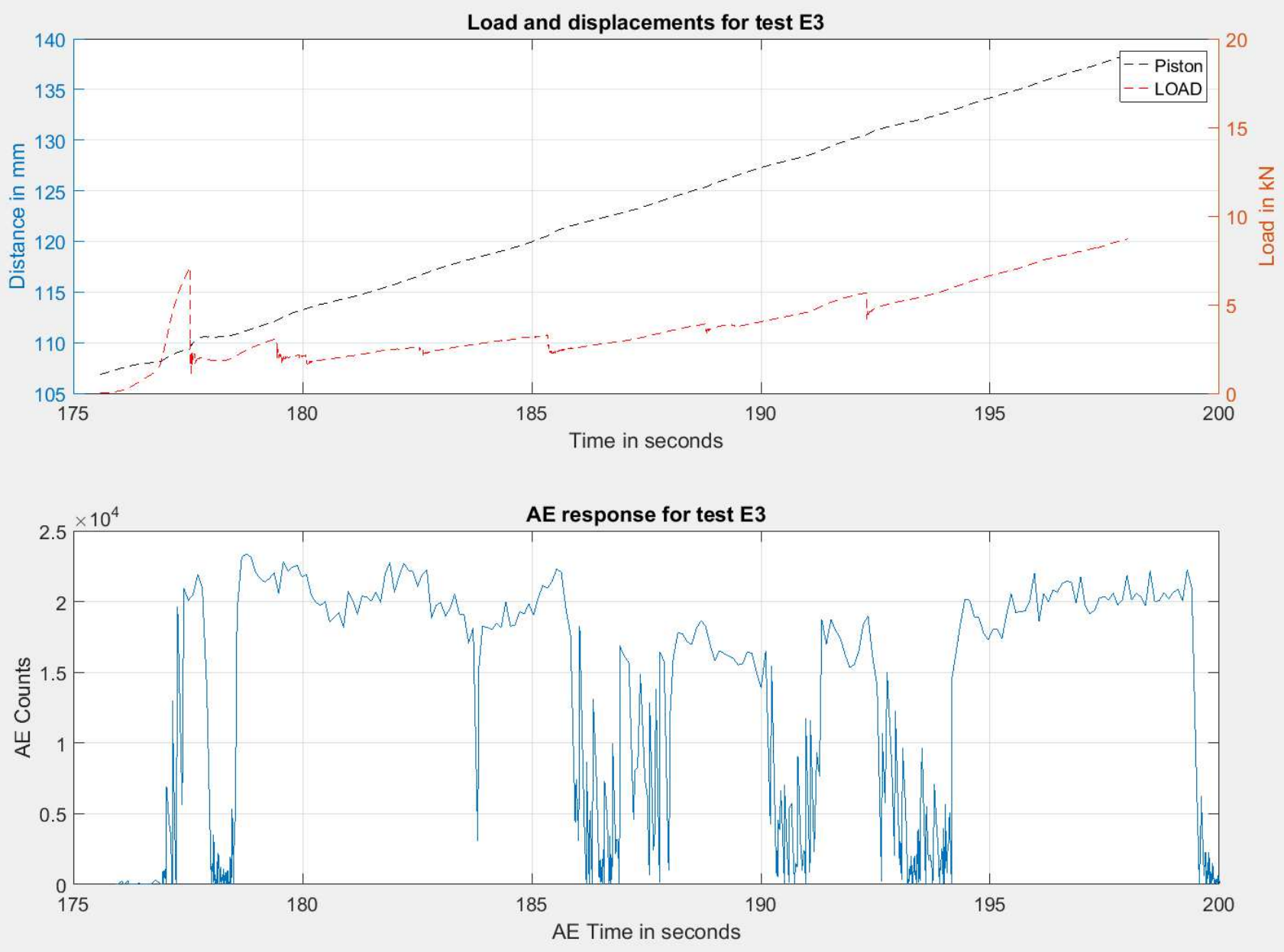
Load and displacements for test E3
Distance in mm
Load in kN
Time in seconds
Piston
LOAD
140
135
130
125
120
115
110
105
20
15
10
5
0
175
180
185
190
195
200
AE response for test E3
×10^4
AE Counts
AE Time in seconds
2.5
2
1.5
1
0.5
0

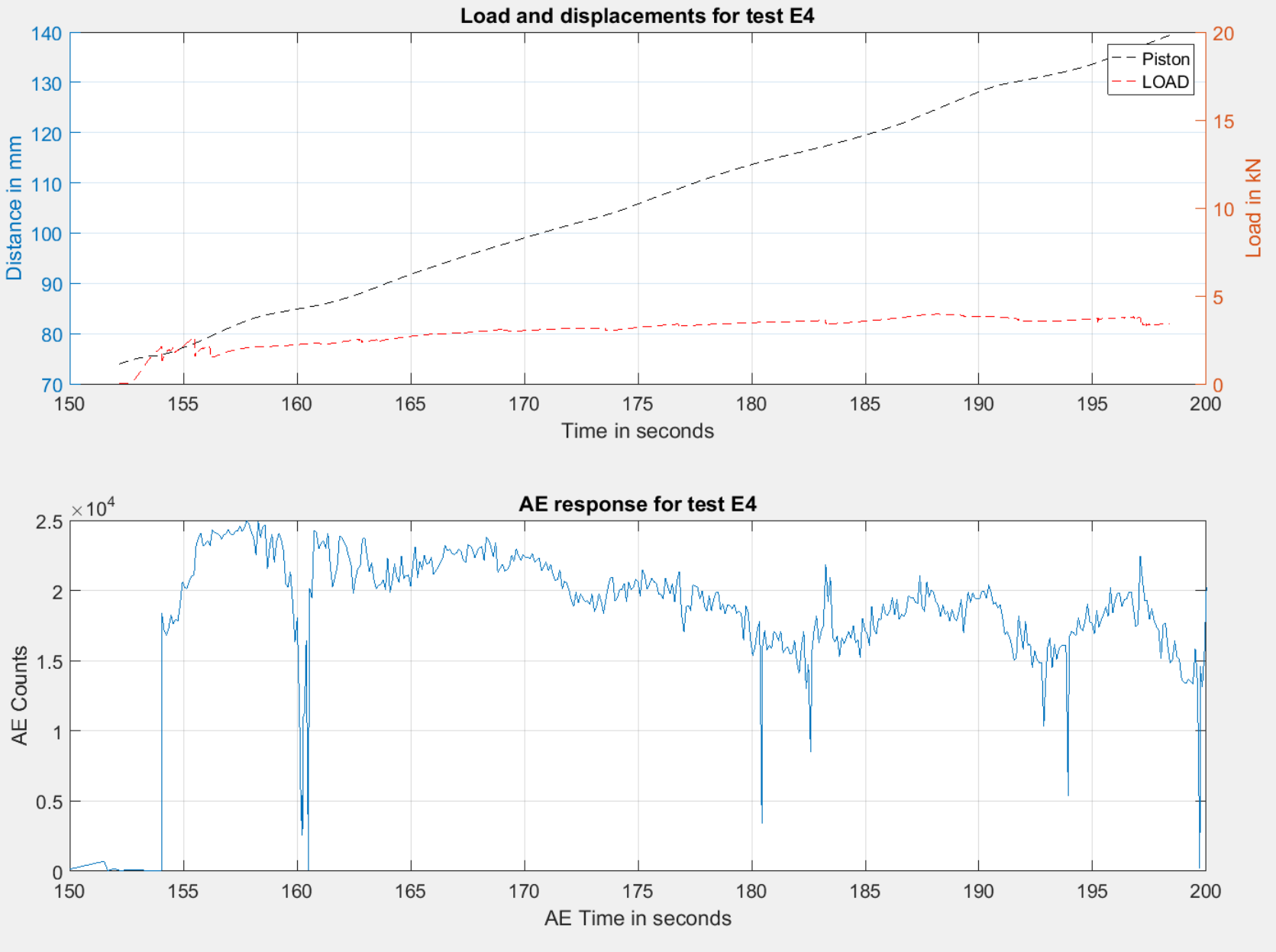
Load and displacements for test E4
Distance in mm
Load in kN
Time in seconds
Piston
LOAD
AE response for test E4
AE Counts
AE Time in seconds

[Test W1 was not recorded, i.e. these data are not available]

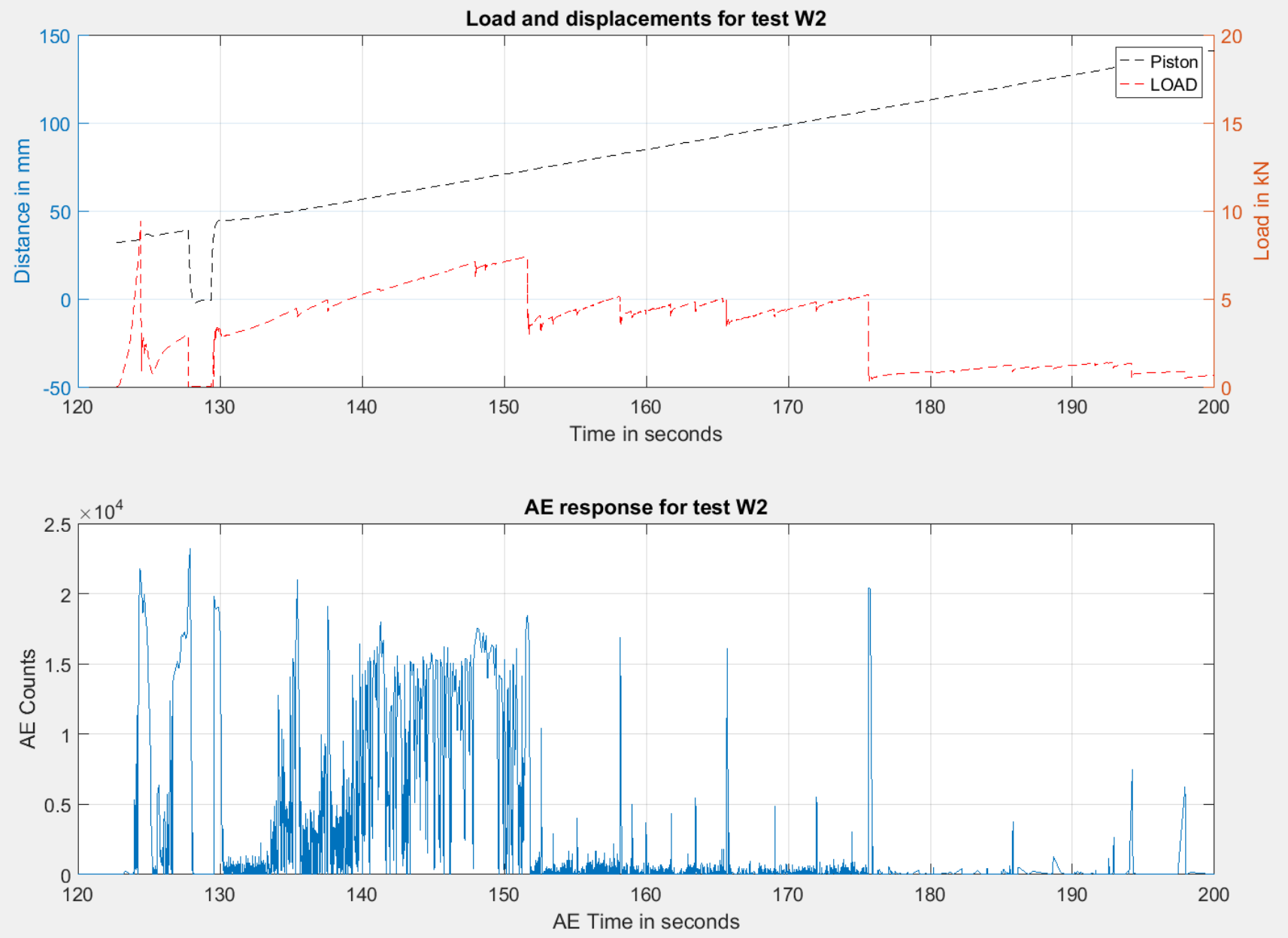
Load and displacements for test W2
Distance in mm
Load in kN
Time in seconds
Piston
LOAD
150
100
50
0
-50
20
15
10
5
0
120
130
140
150
160
170
180
190
200
AE response for test W2
×10^4
AE Counts
AE Time in seconds
2.5
2
1.5
1
0.5
0

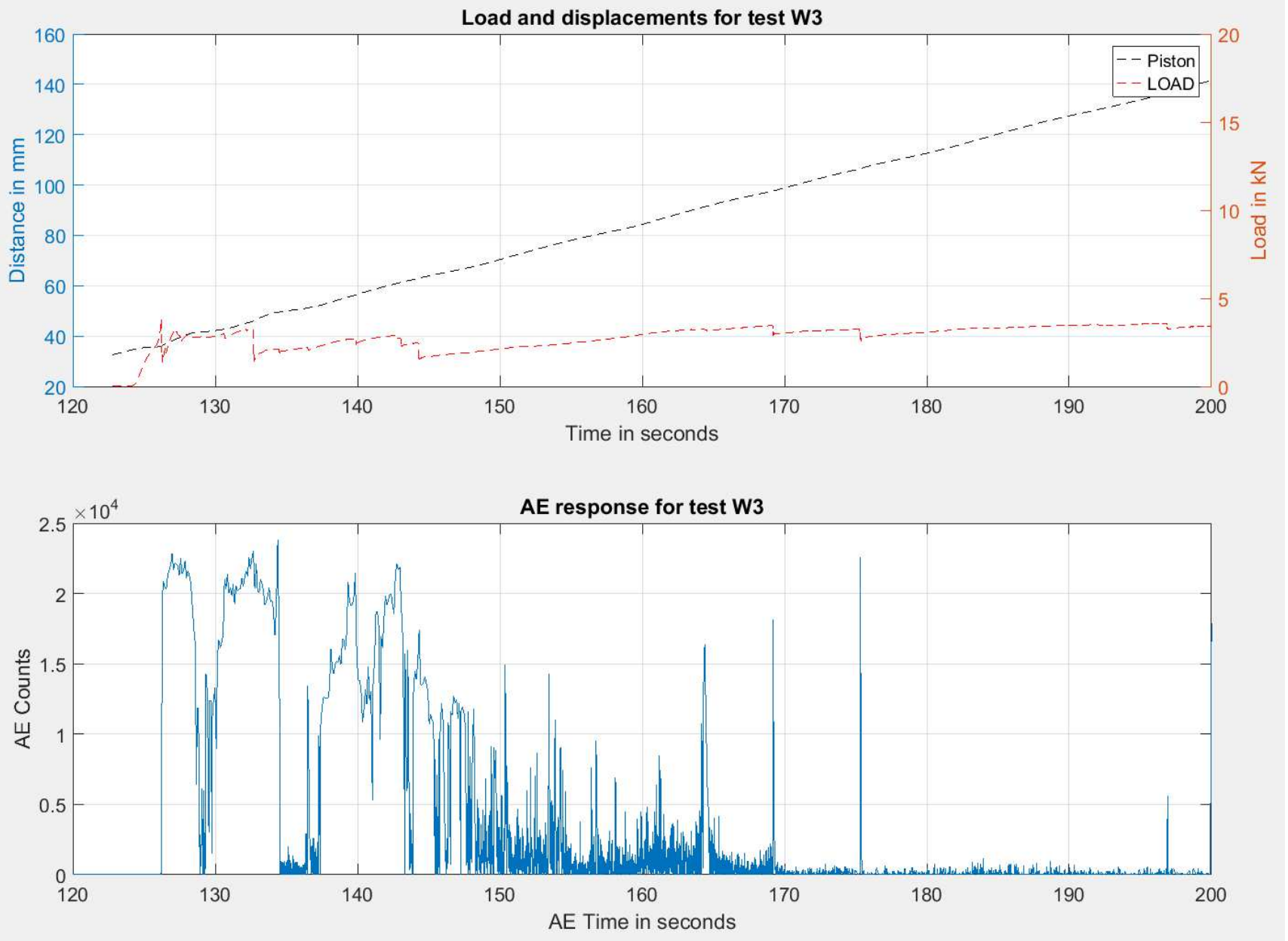
Load and displacements for test W3
Distance in mm
Load in kN
Time in seconds
Piston
LOAD
AE response for test W3
AE Counts
AE Time in seconds

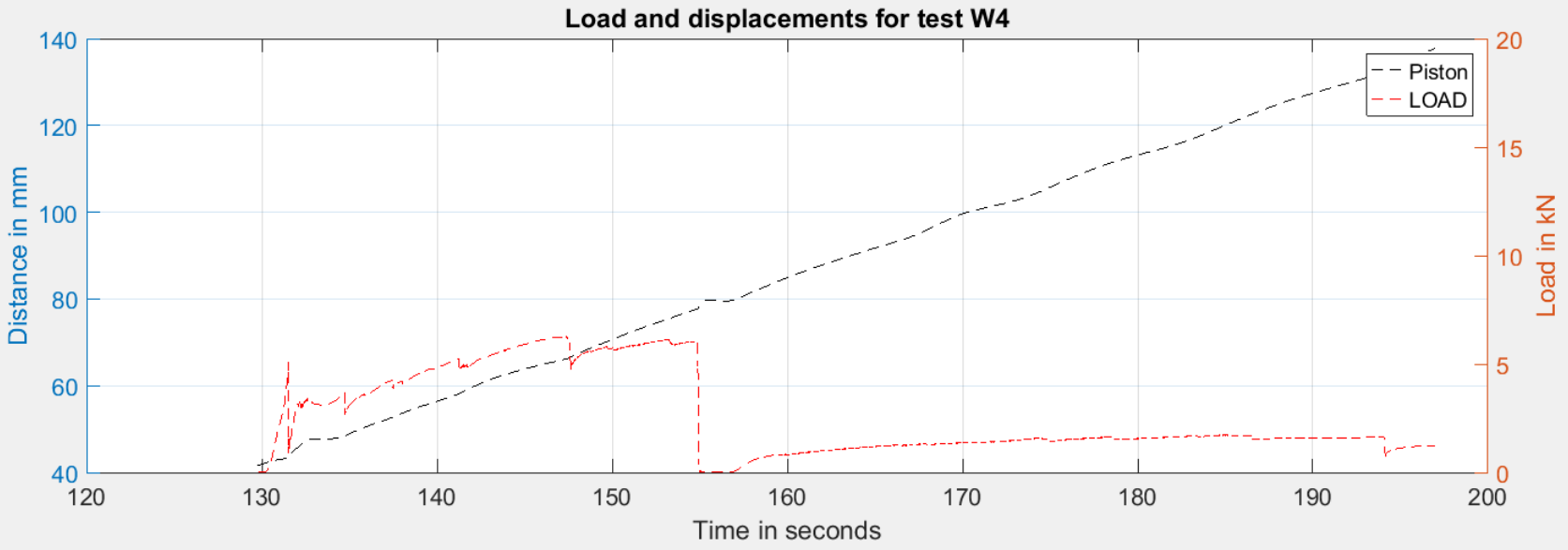
Load and displacements for test W4
Distance in mm
Load in kN
Time in seconds
Piston
LOAD
140
120
100
80
60
40
20
15
10
5
0
120
130
140
150
160
170
180
190
200

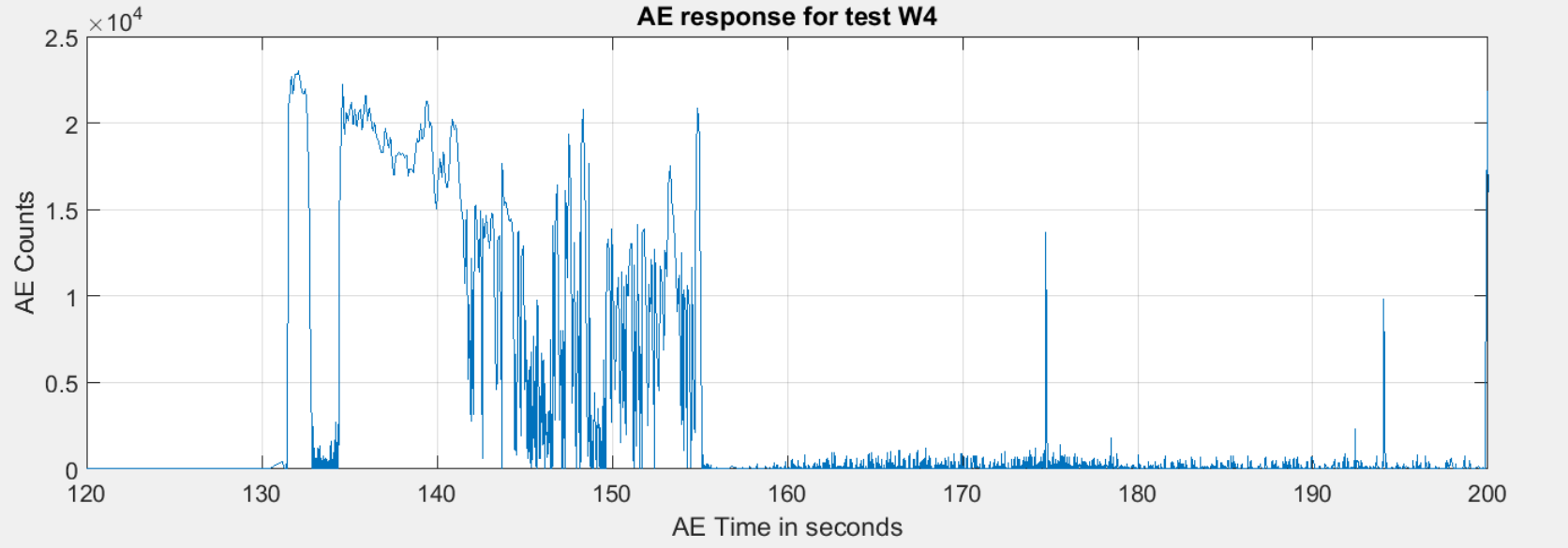
AE response for test W4
×10^4
AE Counts
AE Time in seconds
2.5
2
1.5
1
0.5
0
120
130
140
150
160
170
180
190
200